• U C •

FCTUC FACULDADE DE CIÊNCIAS
E TECNOLOGIA
UNIVERSIDADE DE COIMBRA

DEPARTAMENTO DE
ENGENHARIA MECÂNICA

Shock Impact of Silicon doped Boron Carbide Powders

Submitted in Partial Fulfilment of the Requirements for the Degree of Master in Mechanical Engineering in the speciality of Production and Project

Author

Miguel Gonçalves Rodrigues

Advisors

Professor Cristina Maria Santos

Doctor João Pedro Duarte

Jury

President	**Doctor Ana Paula Bettencourt Martins Amaro** **Professor Auxiliary at University of Coimbra**
Vowels	**Doctor José Manuel Baranda Moreira da Silva Ribeiro** **Professor Auxiliary at University of Coimbra** **Doctor Ricardo António Lopes Mendes** **Professor Auxiliary at University of Coimbra**
Advisor	**Doctor Cristina Maria Gonçalves dos Santos** **Professor Auxiliary at University of Coimbra**

Institutional Collaboration

Imperial College London

Institute of Shock Physics

Coimbra, September, 2015

I have been impressed with the urgency of doing.
Knowing is not enough; we must apply.
Being willing is not enough; we must do.

Leonardo Da Vinci

To my parents.

ACKNOWLEDGEMENTS

The work presented was possible due to the collaboration and support of several persons, who I want to show my gratitude.

To my advisors, Professor Cristina Santos and Doctor João Paulo Duarte, for their invitation, excellent guidance, caring and patience. I am grateful for their insightful knowledge and commitment in aiding my progress with many useful discussions and suggestions.

To Professor José Baranda for the availability, always present to listen and give important and agreed advices, and help in carrying out part of the experimental work.

To ISP, particularly to Doctor William Proud, for receiving me as Erasmus student, and for the opportunity, technical support, help and encouragement without which I would never have come so far.

Finally I would like to dedicate this thesis to my parents, who even without completely understanding what I was doing in London always supported me the best they could. Their courage, energy and love were very important to me during the last five years of my graduation.

For all of you, my thanks.

ABSTRACT

This research is integrated in a line of investigation currently in progress which aims to improve the performance of the boron carbide (B_4C) as a ballistic armour material. In this regard a successful attempt to dope the boron carbide with silicon was done.

The specific goal of the project is to determine the Hugoniot parameters of uniaxially pressed B_4C-Si system. The ceramic material, containing 7%at.Si, was synthesized by Mechanical Allowing (MA) from commercially available Si and B_4C powders in order to obtain a metastable $B_4(C,Si)$ solid solution.

All samples were 7.5 mm in diameter with approximately 1mm thickness and presented theoretical maximum density (TMD) close to 60%. For this purpose, a special die, to optimize the specimen geometry for the launcher, were projected.

The shock behavior of the B_4C-7Si system was done by impact conditions using a gas gun available at the Institute Physics of Shock, Imperial College London. Three plate impact experiments, in the velocities range from 300 to 700 m/s, were conducted and the respective shocked Hugoniot states in the U_s-u_p and p-ν planes were obtained.

When the B_4C-7Si material was shocked a steady shock wave was generated, which propagates at a velocity ranging from 3150 to 3900 m/s and transfers energy into particles which moves at velocities between 245 and 470 m/s after its passage.

The experimental results were compared to those theoretically predicted from Plate Gap and Gruneisen models for porous materials.

Keywords Hugoniot Parameters, Boron Carbide, Dopant, Plate Impact, HetV.

RESUMO

O presente estudo está integrado numa linha de investigação que visa incrementar a performance do carboneto de boro (B_4C) como material para proteção balística. Para o efeito, foi produzido um material monolítico a partir de B_4C dopado com silício.

É objetivo deste trabalho determinar os parâmetros de Hugoniot do sistema B_4C-Si após prensagem uniaxial. O material cerâmico, contendo 7%at.Si, foi obtido por Síntese Mecânica, a partir de pós de Si e de B_4C comercialmente disponíveis, de forma a obter-se uma solução sólida metaestável do tipo $B_4(C,Si)$.

As amostras produzidas possuíam 7,5mm de diâmetro e aproximadamente 1mm de espessura, correspondendo a um valor de densidade teórica máxima de 60%. Foi projetado e fabricado um molde especial para otimizar a geometria das amostras.

O comportamento ao choque do sistema B_4C-7Si foi efetuado em condições de impacto plano, recorrendo a uma arma de gás disponível no *Institute of Shock Physics, Imperial College London*.

Foram realizadas três experiências de impacto, com velocidades na gama 300 - 700 m/s, que permitiram caracterizar a propagação das ondas de choque no material estabelecendo a chamada relação de Hugoniot nos planos U_s-u_p e p-v.

O sistema B_4C-7Si sujeito a impacto, gera uma onda de choque constante que se propaga a uma velocidade entre 3150 e 3900 m/s e a correspondente energia transferida após passagem promove uma velocidade de partículas na gama 245 a 470 m/s.

Os resultados experimentais foram comparados com os teoricamente previstos para materiais porosos recorrendo aos modelos de *Plate Gap* e de *Gruneisen*.

Palavras-chave: Parâmetros de Hugoniot, Carboneto de Boro, Silício, Impacto Plano, HetV.

CONTENTS

LIST OF FIGURES xi
LIST OF TABLES xiii
SIMBOLOGY AND ACRONYMS xv
Simbology xv
Subscripts xvi
Acronyms xvi
1. INTRODUCTION 1
2. STATE OF ART 3
2.1. Material 3
2.2. Low Velocity Impact Testing 6
2.3. Shock Waves 7
2.3.1. Shock Velocity and Particle Velocity 8
2.3.2. Conservation Equations 8
2.3.3. Hugoniot 10
2.4. Porous materials 13
2.5. Velocity measuring techniques 16
2.5.1. VISAR 16
2.5.2. HetV 17
3. EXPERIMENTal CONFIGURATIONs 19
3.1. Plate Impact Experiment 19
3.2. Experimental Setup 20
3.2.1. Alignment 22
3.3. Plate Impact specimen geometry 23
3.4. HetV 25
4. RESULTS AND DISCUSSION 27
4.1. HetV Calibration 28
4.2. Shock Wave Velocity (U_s) 29
4.3. Particle Velocity (u_p) 33
4.4. Hugoniot Parameters 35
4.5. Theoretical Approach 37
5. CONCLUSIONs AND SUGESTIONS 39
6. REFERENCES 41
ANNEX A 45
ANNEX B 51

LIST OF FIGURES

Figure 1.1. Impact of a projectile on a ceramic backed with soft material [4]. 1

Figure 2.1. Representative shock compression profile in ceramic and schematic of brittle shear fracture process within the shock wave front [13]. 3

Figure 2.2. Shear stress and strength Y of boron carbide in the shocked state estimated from re-shock and release experiments [17]. 4

Figure 2.3. Ballistic data on B4C showing an abrupt drop in shear strength at impact pressures of 20-23 GPa [18]. 5

Figure 2.4. A boron carbide ballistic target that comminuted during impact (left) and a HR TEM image of a fragment produced by a ballistic test at impact pressure of 23.3 GPa (right) [19]. The loss of lattice fringes in the band indicates localized amorphization. 5

Figure 2.5. Configuration of plate impact experiments by [17]. 6

Figure 2.6. Computer simulation of a plate impact experiment [23]. 7

Figure 2.7. Shock propagation on a large horizontal plate. 8

Figure 2.8. Conservation of mass and momentum on a shocked block of material. 8

Figure 2.9. Hugoniot representation in U_s-u_p plane. 10

Figure 2.10. Hugoniot representation in p-u_p plane. 11

Figure 2.11. Hugoniot representation in p-u_p plane of a moving object. 11

Figure 2.12. Representation in p-u_p plane of a determined shocked state. 12

Figure 2.13. Aluminium Hugoniot representation in p-$\boldsymbol{\nu}$ -E space [23]. 13

Figure 2.14. Schematic representation of the Plate Gap Model in the t-x plane [25]. 15

Figure 2.15. An typical VISAR configuration [27]. 17

Figure 2.16. A typical Het-V configuration [28]. 18

Figure 3.1.Schematic representation of the launcher (top), launcher (bottom left) and target chamber (bottom right). 19

Figure 3.2. Experimental setup - exploded View. 20

Figure 3.3. Target and its respective components. 21

Figure 3.4. Probes position. 21

Figure 3.5.Target holder alignment. 22

Figure 3.6. a) Optical image of a sample; b) Shock wave paths in the sample. 23

Figure 3.7.Die and its respective components. 23

Figure 3.8.Probe schematic used in this work. 25

Figure 4.1.Moving average trend line of the four signals from each channel in the calibration experiment..... 28
Figure 4.2.Time correction of the channels..... 29
Figure 4.3.Plot signal from the plate impact experiment on Sample #01. 30
Figure 4.4.Plot signal from the plate impact experiment on Sample #02. 30
Figure 4.5.Plot signal from the plate impact experiment on Sample #03. 31
Figure 4.6.Free surface velocity profile of Sample #01. 33
Figure 4.7.Free surface velocity profile of Sample #02. 33
Figure 4.8.Free surface velocity profile of Sample #03. 34
Figure 4.9. Experimental results in the U_s-u_p plane with linear regression of the results of the samples #02 and #03. 35
Figure 4.10. Experimental results and the initial density in the p-ν plane. 36
Figure 4.11. Comparisons of solid boron carbide Hugoniot data [12]. 36
Figure 4.12.Representation of the experimental data and the models of Gruneisen and Thouvenin for porous materials in the p-ν plane. 38
Figure 4.13. Hugoniot results on porous B_4C from Marsh [30] with different initial densities comparisons with results from this report. 38

LIST OF TABLES

Table 1.1. Mechanical properties of Boron Carbide [5]. 2
Table 4.1. Main characteristics of the B_4C-7at.Si samples. 27
Table 4.2. Shock waves arrival times (accuracy better than 5 ns). 32
Table 4.3. Shock Wave velocity. 32
Table 4.4. Experimental data. 34

SIMBOLOGY AND ACRONYMS

Simbology

A – Area

C_0 – Bulk Speed of Sound

d_s – Sample's diameter

E – Internal Energy

e_s – Sample's thickness

E_t – Total energy

m – Mass

p – Pressure

S – Linear Hugoniot slope coefficient

t – Instant of time

t_f – Time of arrival of the shock wave to the end of the sample

t_i – Time of arrival of the shock wave to the sample

u_p – Particle velocity

U_s – Shock wave velocity

V – Velocity

W – Work

Γ – Gruneisen parameter

Δt – Interval of time

λ – Thouvenin parameter

ν – Specific volume

ρ – Density

τ_h – Shear Stress

Y_h – Shear Strength

Subscripts

0 – Not shocked

1 – Shocked

P – Porous material

S – Non porous material

Acronyms

1-D – One Dimensional

2-D – Two Dimensional

CEMUC – Centro de Engenharia Mecânica da Universidade de Coimbra

DEM – Departamento de Engenharia Mecânica

EoS – Equation of State

FCTUC – Faculdade de Ciências e Tecnologia da Universidade de Coimbra

FFT – Fast Fourier Transform

HEL – Hugoniot Elastic Limit

HetV – Heterodyne Velocimeter

HR TEM – High resolution transmission electron microscopy

ICL – Imperial College London

ISP – Institute of Shock Physics

MA – Mechanical Allowing

SEG – Surface Engineering Group

TMD – Theoretical Maximum Density

UC – Universidade de Coimbra

VISAR – Velocity Interferometer System for Any Reflector

1. INTRODUCTION

Much of the early research into the propensity of ceramic-based materials to resist penetration to projectiles occurred back in the 1960s, mostly under the leadership of M. L. Wilkins [1]. Wilkins [2,3] recognized that in order to optimize a two-component ceramic armour system, see Figure 1.1, it is necessary to understand the interaction between the target and projectile.

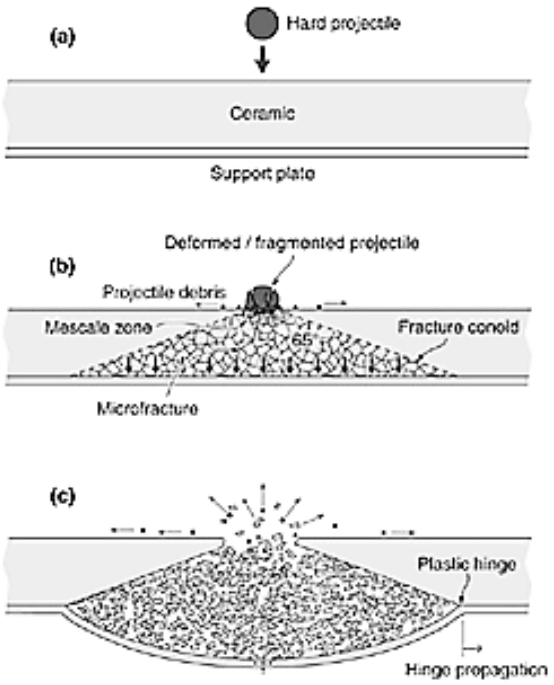

Figure 1.1. Impact of a projectile on a ceramic backed with soft material **[4]**.

The benefit of using ceramic materials, in opposition to metallic materials as the flyer plates, is that the ceramic very rapidly breaks down into small fragments thereby minimizing any collateral damage. This is exceptionally suitable for lightweight armoured vehicles that may be operating in urban zones.

Boron Carbide, usually denoted as B_4C, is a very attractive material for lightweight armour systems due to its low density and ability to retain a high compressive

strength and shear strength under dynamic compression, outstanding its elastic modulus and hardness (see Table 1.1).

Table 1.1. Mechanical properties of Boron Carbide **[5]**.

Knoop hardness (GPa)	Wear resistance (a.u.)	Strength (MPa)	Toughness, K_{1c} (MPa.√m)	Youngs´s modulus (GPa)	Poisson ratio	Shear modulus (GPa)	Density (Kg/m^3)
29 - 35	0.4 - 0.422	300 - 500	1.512	360 - 460	0.17	158 - 188	2.52

However, practical use of B_4C as armor material for high velocity projectiles is limited [6]. This is due to its anomalous glass-like behavior, which has been linked to stress-induced structural instability in one of its polymorphs, the B_{12}(CCC). Theoretical calculations obtained by other research workers [7] suggest that the formation of weaker crystalline configurations could be suppressed by silicon doping.

This research work is part of an ongoing collaboration between the Institute of Shock Physics (ISP) at Imperial College London (ICL) and the Mechanical Engineering Department of Coimbra University (CEMUC and ADAI Centres) and aims improving the ballistic properties of B_4C by doping with lightweight materials.

In this context, the B_4C-Si system was selected.

The material preparation were done in DEM, Coimbra, by other colleague in their experimental work thesis [8,9] while the Hugoniot parameters, which relate the particle velocity with the shock wave velocity into material, were measured by plate impact experiments using the ISP's 13 mm bore single-stage meso-scale launcher, available at the ISP, London.

The structure of the present dissertation contains five chapters.

The second chapter is dedicated to the literature survey concerning the ceramic material and the plate impact facility. A brief introduction to the shock waves concept is also presented. In the third chapter all the experimental work is presented, mainly the material characteristics and the procedures for the plate impact tests. The results obtained including the theoretical are fulfilled in the fourth part. Finally, the fifth chapter cover the main conclusions of the work.

2. STATE OF ART

In order to gather all knowledge necessary for this study it was reviewed some previous articles of plate impact experiments with a special focus on the ones on boron carbide and silicon carbide, two high-strength ceramics. Since the material was tested in its porous form (uniaxial press of powders) a review concerning porous material *vs* solid material was done. Also the study about shock waves, shock Hugoniot and measuring techniques for high impact experiments will be presented.

2.1. Material

Extensive analysis of shock profiles in different ceramic specimens such as Al_2O_3, SiC and B_4C has been conducted by Grady [10-13]. Figure 2.1 shows a schematic representation of a reasonable physical model of the shear fracture process within the shock front of a ceramic under compressive stress. First, the specimen is subjected to a quick elastic shock reaching rapidly the Hugoniot Elastic Limit. The HEL corresponds to the maximum uniaxial dynamic stress that the material can withstand elastically, and is the key parameter that determines the strength of a ceramic under shock loading.

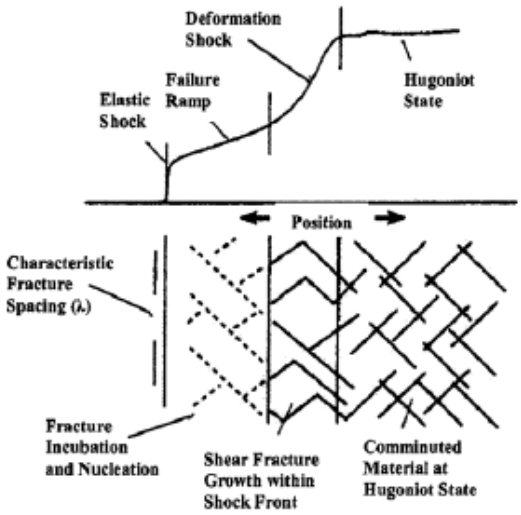

Figure 2.1. Representative shock compression profile in ceramic and schematic of brittle shear fracture process within the shock wave front **[13]**.

In the high-strength ceramic, Figure 2.1, elastic stress of 2-20 GPa is reached with only 2-5% of shear strain, then, during the failure ramp the material quickly changes its elastic volumetric compressibility and finally, if premature failure does not occur, a drastic inelastic shear deformation and shear fracture growth begins.

The boron carbide (B_4C) is a fascinating ceramic material due to its low density and high strength making it ideal for armour applications. The shock behaviour of this material has been studied through the years by several researchers [6,10,14-16]. These studies showed that the HEL of B_4C is 14-19 GPa, which is the highest report for a ceramic material [10]. Such a property would suggest that boron carbide could withstand high pressures. However, laboratory experiments reveal that the performance of boron carbide at high velocity and high pressure impacts is much lower than expected if one takes into account excellent static mechanical properties of B_4C (see Table 1.1). The small amount of plasticity above the HEL is thought to be the primary reason for failure of boron carbide at lower than expected impact pressures

The shear stress τ_h and shear strength Y_h of boron carbide in the shocked state are shown in Figure 2.2 [17]. In contrast to a similar relationship in a typical ceramic material, the shear stress and strength in B_4C fall off rapidly above HEL, indicating premature failure of the material as the shock stress reaches a threshold value of 20 - 25 GPa.

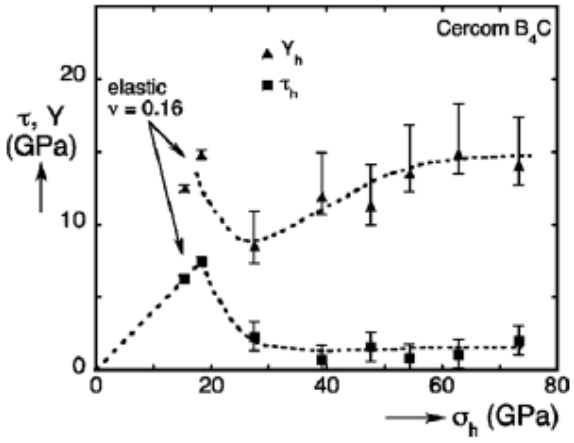

Figure 2.2. Shear stress and strength Y of boron carbide in the shocked state estimated from re-shock and release experiments **[17]**.

An identical abrupt drop in the shear strength of boron carbide at impact pressures of 20-23 GPa has been reported in ballistic testing, as illustrated in Figure 2.3 [18].

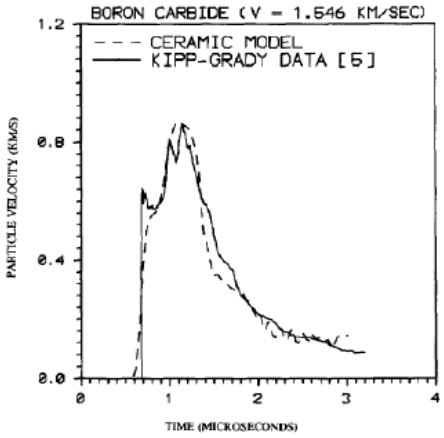

Figure 2.3. Ballistic data on B4C showing an abrupt drop in shear strength at impact pressures of 20-23 GPa **[18]**.

The damage mechanism responsible for such failure has been assessed by Chen *et al*. [19]. High resolution transmission electron microscopy (HR TEM) analysis of B_4C ballistic targets subjected to supercritical impact velocities and pressures (in excess of 20-23 GPa) revealed the formation of 2-3 nm wide intergranular amorphous bands that occur parallel to specific crystallographic planes and contiguously with apparent cleaved fracture surfaces (see Figure 2.4). At subcritical impacts, the amorphous bands were never observed; instead a relatively high density of stacking faults and micro-twins suggested plastic deformation of the material under shock loading [19].

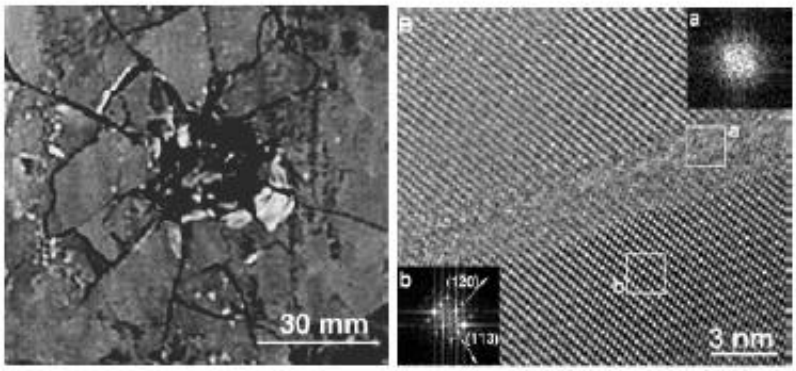

Figure 2.4. A boron carbide ballistic target that comminuted during impact (left) and a HR TEM image of a fragment produced by a ballistic test at impact pressure of 23.3 GPa (right) **[19]**. The loss of lattice fringes in the band indicates localized amorphization.

An attempt to improve the ballistic properties of B_4C by doping with others lightweight materials was made by [8,9]. These works were integrated in the same line of present research working, aiming to determine the ballistic performance of monolithic ceramics in the B4C-M, M = Al, Mg, Si systems.

2.2. Low Velocity Impact Testing

The most common practice to determine the properties of high-strength materials is with plate impact experiments conducted using projectile launchers (powder gun, single-stage and two-stage light gas guns).

Probably the three most important properties that can be gleaned from plate-impact test are:

i) the dynamic shear strength, ii) the Hugoniot Elastic Limit (HEL) and iii) the spall strength.

The HEL (which represents the yield strength under 1-D strain conditions, in metals at least) is the transition from elastic to inelastic behaviour as a compression wave propagates through the material. However, in ceramics it was widely accepted that this is the point that microcracking began. This viewpoint has been challenged by some researchers who have found evidence of damage within the elastic region [20,21].

The studied experiments to determine the properties of B_4C and SiC done by several researchers [6,11,17,22] follows the configuration illustrated in Figure 2.5 and were performed with a range of velocities from 0,1 km/s to 7 km/s.

Plates with 28-100 mm diameter and 1.2-4 mm of thickness of the same ceramic, or a high density metal (Copper, Tantalum) were mounted on the projectile and caused to impact stationary target plates of the test ceramic. The impactor in some of the experiments in order to induce re-shock or release behaviour was backed with a high or low impedance material. The target 3-10.5 mm thick is backed by a lithium fluoride window (LiF), which was the surface in contact with the sample diffused with vapour deposited aluminium.

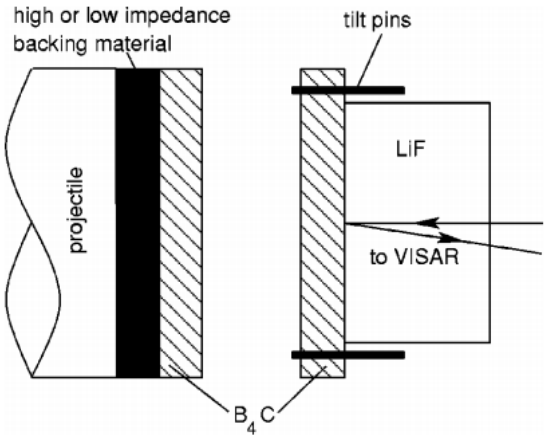

Figure 2.5. Configuration of plate impact experiments by **[17]**.

Projectile velocity was measured in some cases by electrical self-shortening pins and others by an optical system with accuracies better than 0.5% and 0.2% respectively, additionally pins were used to measure the impact planarity. The particle velocity history at the target-window interface is measured using velocity interferometer system to any reflector (VISAR) with accuracy better than 2%.

All the experiments were conducted with dimensions to assume uniaxial strain conditions for the central region of the sample for its duration.

2.3. Shock Waves

To an easier understand of the shock wave's behaviour this study was made for the condition of one dimensional, (1-D) configuration. This imply that all the variations (say pressure, density etc.) take place in one direction only. Imagine the situation two half spaces collide with each other horizontally, just after collision the state of the material will only vary with distance in the same direction of the impact.

In a real experiment it is also possible to produce 1-D conditions although for a finite interval of time. On the impact of a flat plate into a cylindrical target, as shown in Figure 2.6, it is possible to observe a 1-D condition in the centre of the cylinder along its axis for a brief interval of time. Eventually a release wave from the outer surface reaches the axis and the 1-D conditions no longer apply.

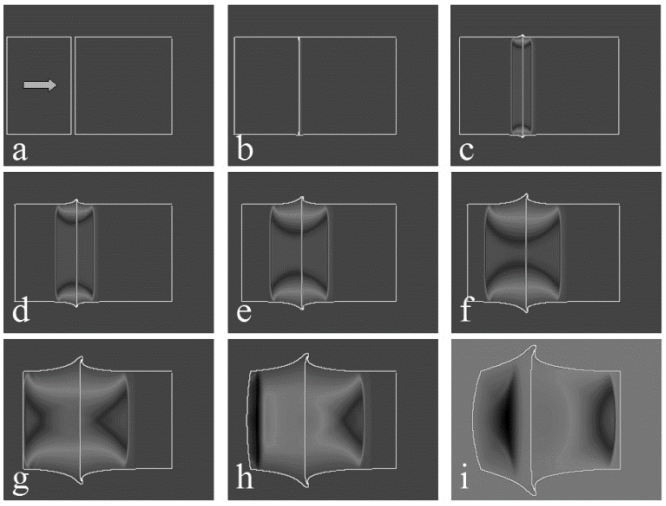

Figure 2.6. Computer simulation of a plate impact experiment **[23]**.

2.3.1. Shock Velocity and Particle Velocity

The Figure 2.7 shows successive stages of a shock propagation in a vertical line of particles from a large horizontal plate impacted on its lower surface by an infinite half space rigid material. The shock wave propagates through the material to the top and then reflect off the free surface. The illustration shows that after a shock reaches an initial-at-rest free surface, the surface gains velocity of twice the particle velocity.

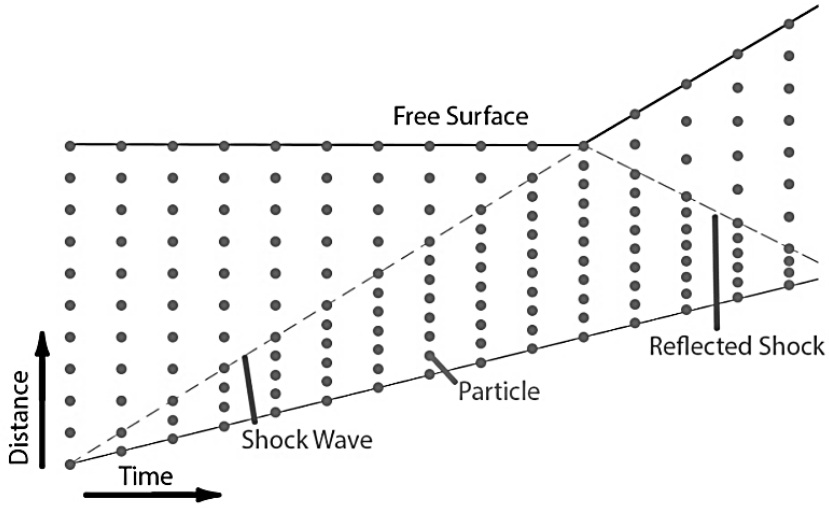

Figure 2.7. Shock propagation on a large horizontal plate.

2.3.2. Conservation Equations

Consider a block of material shocked from its left hand face, Figure 2.8. The time instant $t=0$ represents the moment of impact and the time instant $t=\Delta t$ a moment later. The conservation laws of mass, momentum and energy can be applied to the material.

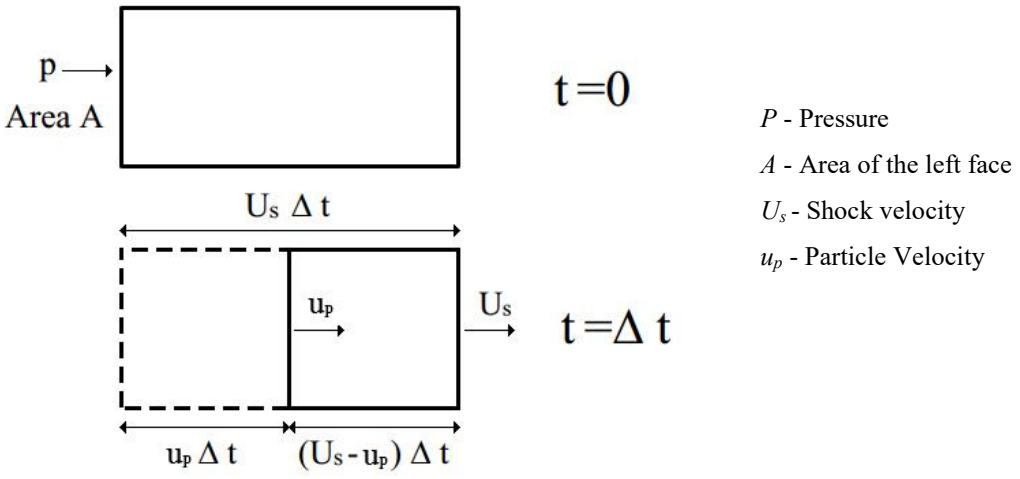

Figure 2.8. Conservation of mass and momentum on a shocked block of material.

Considering the law of the mass conservation, the mass before (m_0) and after (m_1) the impact has the same value, that is:

$$m_0 = m_1 \Leftrightarrow \tag{2.1}$$

$$\rho_0 A U_s \Delta t = \rho A \left(U_s - u_p\right) \Delta t \Leftrightarrow \tag{2.2}$$

$$\rho_0 U_s = \rho \left(U_s - u_p\right), \tag{2.3}$$

Where,

ρ_0 - initial density of the material

ρ - density of the material after shocked.

By the law of conservation of momentum, it can be written:

$$p = \frac{m}{A}\frac{dV}{dt} \tag{2.4}$$

$$p = \frac{\rho_0 U_s A \Delta t u_p}{A \Delta t} \tag{2.5}$$

$$p = \rho_0 U_s u_p, \tag{2.6}$$

Where, V is the velocity.

By the law of conservation of energy, the work (W) done by the applied force is equal to the specific energy gained by the particles (E_t), that is:

$$W = (pA) \times \left(u_p \Delta t\right) \tag{2.7}$$

$$E_t = \rho_0 U_s A \Delta t \left(E + \frac{1}{2} {u_p}^2\right) \tag{2.8}$$

Using the equation for the pressure (2.2) from the conservation of momentum it is possible to obtain the following equation for the specific internal energy E:

$$E = \frac{1}{2} {u_p}^2 \tag{2.9}$$

Other useful equations can be obtained by combining the equations (2.3), (2.6) and (2.9) in different ways.

The derivations were made assuming that the material is initially at zero pressure, internal energy and particle velocity. A similar analyse can be performed for non-zero initial conditions.

2.3.3. Hugoniot

One of many representations of the Hugoniot can be found by the line passing through several shocked states of a material represented in the U_s-u_p plane. It was found experimentally that for many materials that representation is a straight line in the U_s-u_p plane, Figure 2.9. In this case the equation of the Hugoniot may be written as:

$$U_s = C_0 + Su_p, \tag{2.10}$$

With

C_0 - bulk sound speed

S - linear Hugoniot slope coefficient of the material

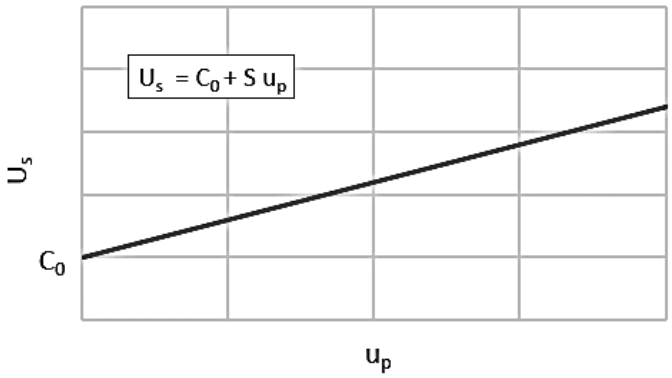

Figure 2.9. Hugoniot representation in U_s-u_p plane.

Another representation of the Hugoniot can be found in the p-u_p plane, Figure 2.10, by combining the equations (2.6) and (2.10) giving rise to:

$$p = \rho_0(C_0 + Su_p)u_p, \tag{2.11}$$

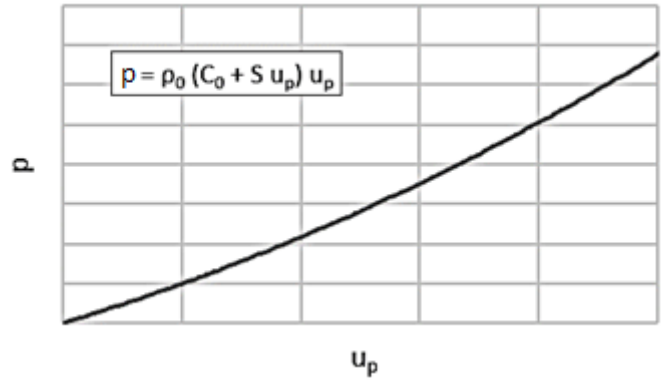

Figure 2.10. Hugoniot representation in p-u_p plane.

This is valid for an initial-at-rest material but since we are studying interactions between objects at least one is moving. Therefore it is important to know how to construct the Hugoniot of a moving object. The simplest case is when an object is moving in the positive direction with velocity *V*. All the particles in the object are initially moving with velocity *V*. This means the particle velocity is *V*, so the Hugoniot equation in the p-u_p plane, Figure 2.11, will assume the following equation:

$$p = \rho_0 \left(C_0 + S\left(V - u_p\right)\right)\left(V - u_p\right), \tag{2.12}$$

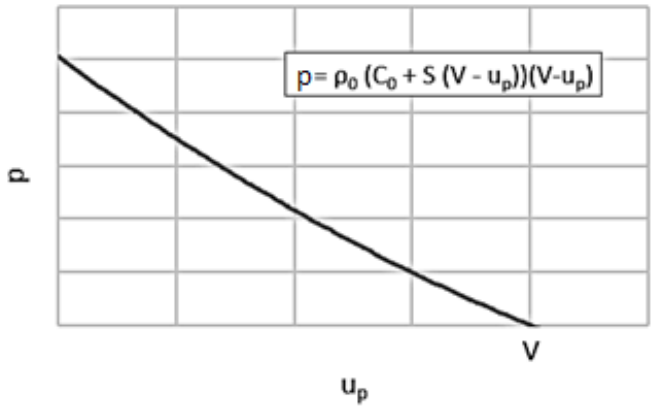

Figure 2.11. Hugoniot representation in p-u_p plane of a moving object.

The Rayleigh Line is a useful construction which helps to illustrate and analyse hydrodynamic situations. It is a straight line that can be represented in the p-u_p plane and is given by the equation (2.6) when the shock velocity and the initial density of the material is

known. Combined with the Hugoniot equation (2.11) it is possible to deduce the value for pressure and particle velocity in the wave, Figure 2.12.

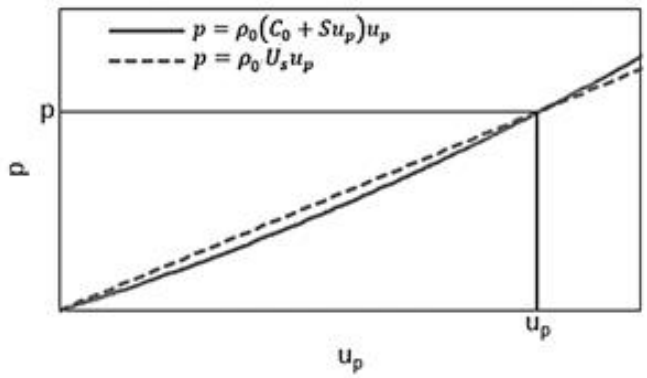

Figure 2.12. Representation in p-u_p plane of a determined shocked state.

The projection of the Hugoniot in the p-υ plane can be defined by joining the equations (2.3), (2.6) and (2.9) giving rise to:

$$p(v) = \frac{{C_0}^2(v_0 - v)}{\left(v_0 - S(v_0 - v)\right)^2}, \tag{2.13}$$

Where,

v_0 - initial specific volume

$p(v)$ - pressure along Hugoniot as a function of specific volume v.

The Hugoniot representation in the E-ν plane where $E(v)$ is the energy along Hugoniot as a function of specific volume v is done by:

$$E(v) = \frac{1}{2}p_h(v)(v_0 - v) \tag{2.14}$$

that is,

$$E(v) = \frac{1}{2}\frac{{C_0}^2(v_0 - v)^2}{\left(v_0 - S(v_0 - v)\right)^2} \tag{2.15}$$

A more complete form to express the Hugoniot is to represent it in the Equation of State (EoS) in the p, v, E space, $p=f(v,E)$. An example of a typical EoS surface is shown in the Figure 2.13. The thick line shows the form of Hugoniot.

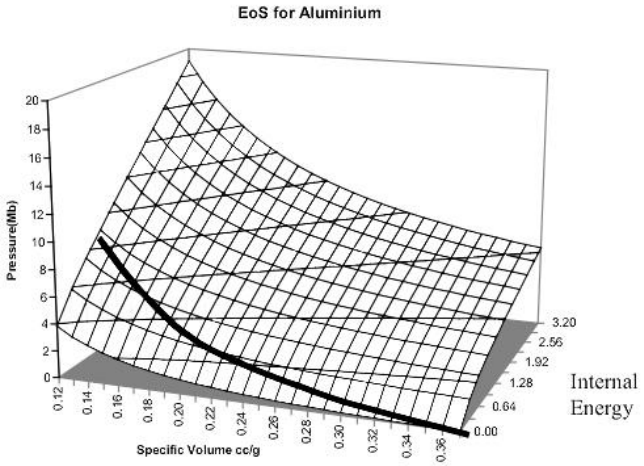

Figure 2.13. Aluminium Hugoniot representation in p-$\boldsymbol{\nu}$ -E space **[23]**.

The mathematical equation for the surface known as The Linear Gruneisen EoS [24] is commonly written as:

$$p = P(\nu) + \frac{\Gamma(\nu)}{\nu}\big(E - E(\nu)\big), \tag{2.16}$$

Where the $\Gamma(\nu)$ Gruneisen gamma given by the following equation:

$$\Gamma = \nu\left(\frac{\delta p}{\delta E}\right)_{\nu} \tag{2.17}$$

2.4. Porous materials

There are several models for the determination of the Hugoniot of porous materials starting with the properties of the solid material. One that is probably the most applied model starts from the Gruneisen equation (2.16). By assuming that the subscript *s0* and *s1* stands for the solid material in the initial and final stages, respectively, and *p0* and *p1* for the case of porous material it is possible to rewrite the equation for a solid material as follow:

$$p_{s0} = p_{s1} + \frac{\Gamma(\nu_{s1})}{\nu_{s1}}\big(E_{s0} - E(\nu_{s1})\big) \tag{2.18}$$

While for a porous material, it becomes:

$$p_{p0} = p_{p1} + \frac{\Gamma(v_{p1})}{v_{p1}}\left(E_{p0} - E(v_{p1})\right) \tag{2.19}$$

By matching the equations to the initial internal energy and when $v_{s1}=v_{p1}$ the equation takes the following form:

$$E_{p1} - E_{s1} = (p_{p1} - p_{s1})\frac{v_1}{\Gamma}, \tag{2.20}$$

with v_1 as the final specific volume for both porous and solid materials.

The equations (2.3), (2.6) and (2.9) can be rearranged and combines to form the following equations.

For a solid material:

$$E_{s1} = \frac{p_{s1}}{2}(v_{s0} - v_{s1})^2 \tag{2.21}$$

Thus, the correspondent equation for a porous material:

$$E_{p1} = \frac{p_{p1}}{2}\left(v_{p0} - v_{p1}\right)^2 \tag{2.22}$$

From the combination of equations (2.20), (2.21) and (2.22) it is possible to obtain the expression for the pressure in the final stage of the porous material, that is:

$$p_{p1} = \frac{p_{s1}\left(\frac{\Gamma(v_{s0} - v_1)}{2v_1} - 1\right)}{\left(\frac{\Gamma(v_{p0} - v_1)}{2v_1} - 1\right)} \tag{2.23}$$

By replacing p_{s1} from equation (2.13) it is possible to obtain the expression to determine the Hugoniot in the p-ν plane for a porous material, knowing the initial density of the solid and porous material and the Hugoniot and Gruneisen parameters of the solid material.

$$p_{p1} = \frac{(\Gamma(v_{s0} - v_1) - 2v_1){C_0}^2(v_{s0} - v_1)}{(\Gamma\left(v_{p0} - v_1\right) - 2v_1)(v_{s0} - S(v_{s0} - v_1))^2} \tag{2.24}$$

Jacques Thouvenin also developed a model that can roughly determine the Hugoniot for porous materials known by Plate Gap Model [25].

The model is focused in how the shock wave propagates in the material. The objective is to analyse the shock wave in a uniaxial model and for that it was assumed that the material is formed by several solid plates with thickness a and spaced within another with a distance b, assuring that the densities of the model and the porous material are the same.

For better understanding, the model presented by Thouvenin is schematically presented in the Figure 2.14

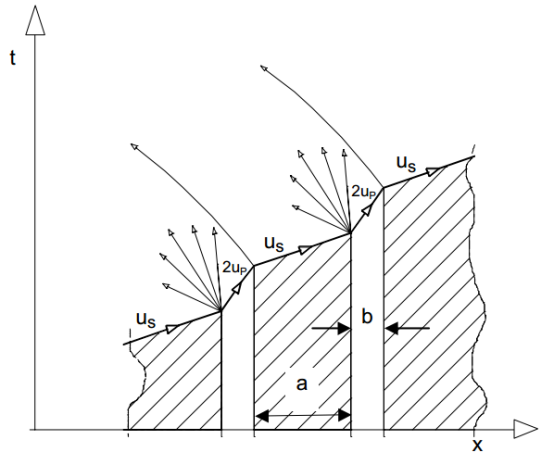

Figure 2.14. Schematic representation of the Plate Gap Model in the t-x plane **[25].**

The propagation, in this model, is associated to the consecutive impact of the plates that causes the shock wave to go through the material. The shock wave travels within the plate with velocity of U_s and reaching the free surface it acquires velocity of approximately two times the particle velocity in the direction of the second plate. The plates shock and the process is repeated.

The expression for the shock wave velocity U_{sp} and particle velocity u_{pp} in the porous material can be obtained with the relation between the time of propagation of the shock waves in the plates and the free surface in the space between the plates.

$$\frac{1}{U_{sp}} = \frac{\lambda}{U_s} + \frac{1-\lambda}{2u_p} \tag{2.25}$$

$$\frac{1}{u_{pp}} = \frac{\lambda}{u_p} + \frac{1-\lambda}{2u_p} \tag{2.26}$$

Being λ, a parameter that relates ρ_p and ρ_s the densities of the porous and solid materials respectively, given by:

$$\lambda = \frac{a}{a+b} = \frac{\rho_p}{\rho_s} \tag{2.27}$$

The relation p, ν calculated from the values of U_{sp} and u_{pp} with the conservation equations was proven to be true by Hofmman *et al*. [26].

2.5. Velocity measuring techniques

There are a few techniques that can be used to determine the velocity history of a surface. The most commonly used for plate impact experiments is the velocity interferometer system for any reflector (VISAR) [27]. Recently a new technique emerged, heterodyne velocimeter (HetV) [28].

2.5.1. VISAR

It works by measuring the minute Doppler shift in light frequency given to a laser beam as it is reflected from a moving surface with an interferometer. The Doppler shift produces light fringes in the interferometer, and the number of fringes is proportional to the surface velocity. The data consists of recordings of the light intensity outputs from the VISAR interferometer as a function of time, in which each complete oscillation of the light intensity corresponds to one light fringe. To obtain a velocity in function of time record for the surface is necessary to count the number of light fringes up to any given time, multiply it by the Velocity-Per-Fringe constant of the interferometer and repeat this process for each time increment.

Velocities can be determined with accuracy better that 2% in the range from a fraction of meter per second to thousands of meters per second and with a sub-nanosecond resolution. The surface does not need to be mirror polished and changes in its reflectivity or in background light have no effect on the derivation of velocity. The system requires no calibration and measurements.

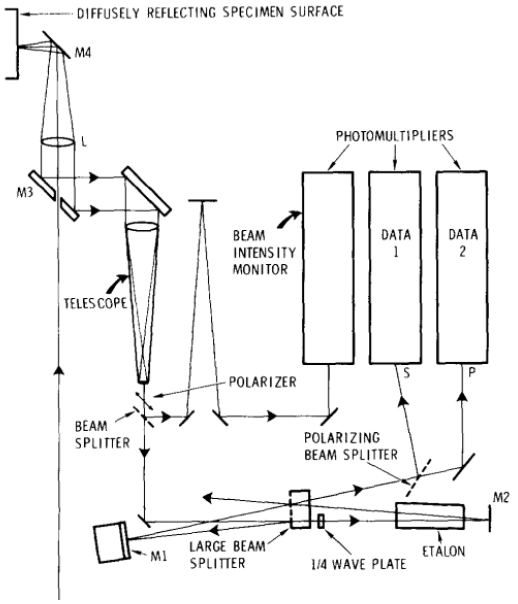

Figure 2.15. An typical VISAR configuration **[27]**.

2.5.2. HetV

By mixing together a portion of the Doppler-shifted light and an equivalent amount of non-Doppler-shifted light it is generated a beat signal proportional to the velocity. The heart of our HetV design is based upon a fiber optic component called a 3-port circulator. The 3-port circulator has the property that light injected into port 1 will be emitted out port 2, and light injected into port 2 will be emitted out port 3. We connect our fiber laser onto port 1, our probe onto port 2, and our detector onto port 3. A fiber transports the light from the laser to the experiment, at its end a probe containing a lens is used to launch the light onto the moving surface and collect a reasonable amount of light reflected from the surface. The Doppler-shifted light is transported by fiber to the detector. The non-Doppler-shifted light is sent directly to the detector and is obtained by the reflection in the fiber end face inside the probe. The beat signal is recorded into a fast digitizer. The maximum velocity is limited by the bandwidth of the electronics and the sampling rate of the digitizers and the record length is limited by the amount of memory contained in the digitizers.

A sliding Fast Fourier transform (FFT) is used in the beat signal data to obtain the frequency vs time information that is directly related with the velocity.

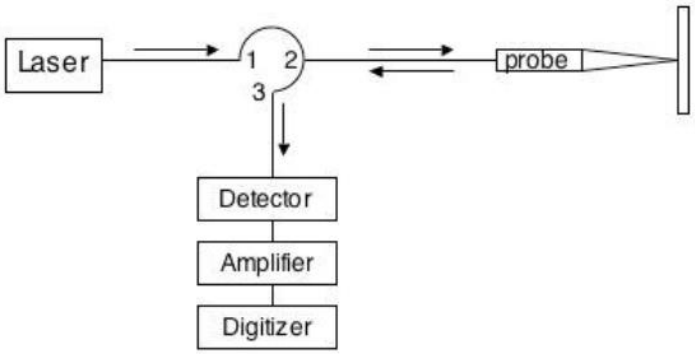

Figure 2.16. A typical Het-V configuration **[28]**.

3. EXPERIMENTAL CONFIGURATIONS

3.1. Plate Impact Experiment

Plate Impact testing was conducted at the Imperial College London using the ISP's 13 mm bore single-stage meso-scale launcher. The launcher consists of two gas tanks, a breach, a barrel, a target chamber, and an expansion tank, see top image in Figure 3.1. Projectile velocities from 100-900 m/s can be achieved by the expansion of helium through its 3 m long barrel.

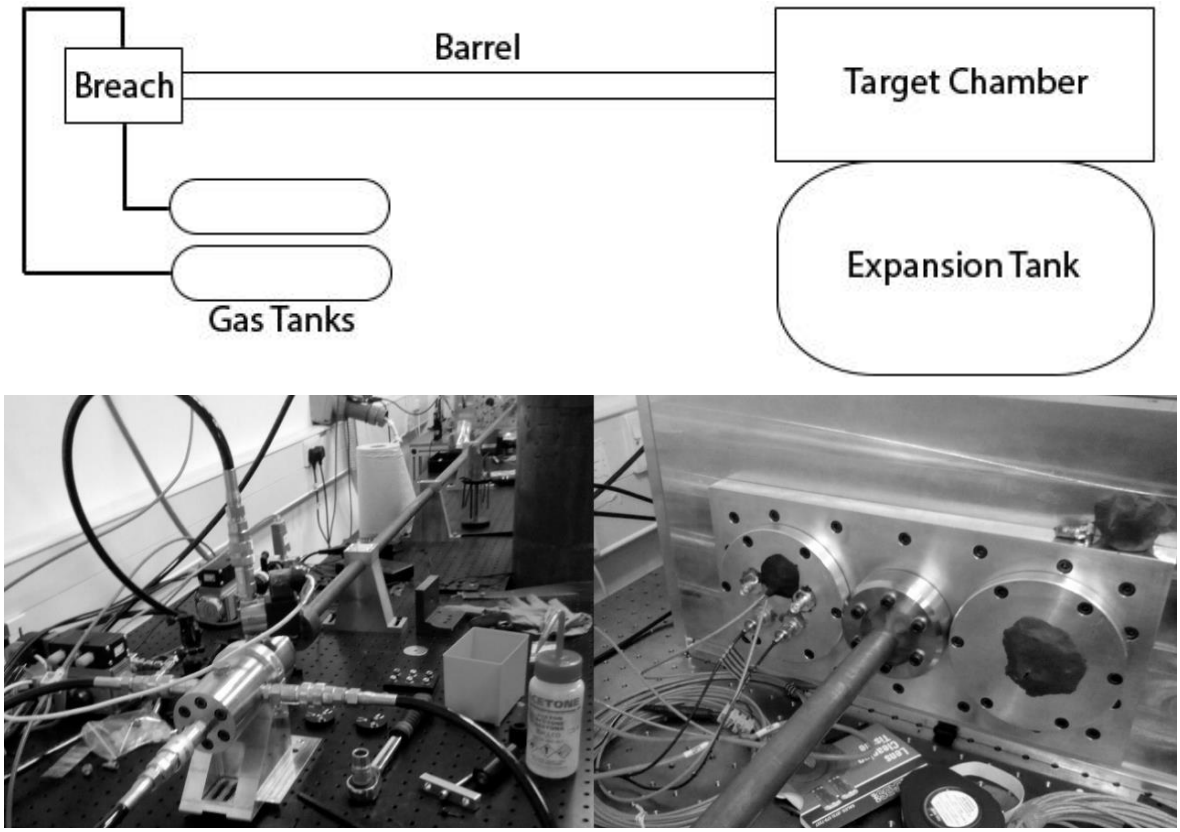

Figure 3.1. Schematic representation of the launcher (top), launcher (bottom left) and target chamber (bottom right).

3.2. Experimental Setup

The experimental setup can be divided in three main parts, as is shown in the Figure 3.2.

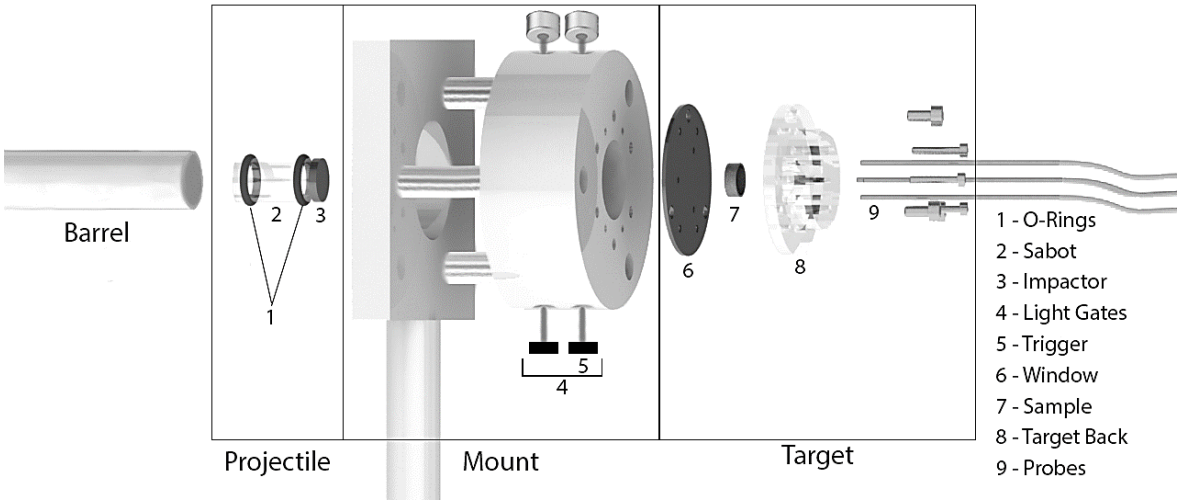

Figure 3.2. Experimental setup - exploded View.

The projectile that will be propelled by the launcher at different velocities. The adjustable mount that serves to align the target perfectly planar to the impactor. And for last the target that holds the sample and the HetV probes.

In the projectile the impactor was set in the sabot with epoxy. The two o-rings are to assure the projectile is fit tight in the barrel without gas leaking from the sides for all the expansion energy of the gas to be used as propellant. To create sufficient pressure in the target the impactor was made of oxygen free high conductivity copper a high density metal with minimal impurities in order to produce a good and clean shock wave. Its face was lapped and polished flat to 1 μm . The sabot was made of PMMA a light material in order for the project to reach high velocities.

To measure the impactor velocity it was attached two light gates to the mount immediately before the target. A Tektronix DPO7254C Digital Phosphor Oscilloscope with a bandwidth of 2.5GHz and sampling rate up to 40GS/s recorded the times at the projectile passes through the light gates allowing velocities to be calculated. Distances between the light gates were accurately measured beforehand.

It was necessary to designed and manufactured the target to hold the sample and the probes of this recent measurement technique, Figure 3.3, the 2D technical drawings are

in the Annex B. The target is constituted by a window and target back part 1 and 2. The window made of the same material as the impactor to avoid alterations in the shock wave had its faces lapped and polished flat to 1 μm and were parallel within one in 10 μm. The target back is made of PMMA to be cheap and of easy manufacturing.

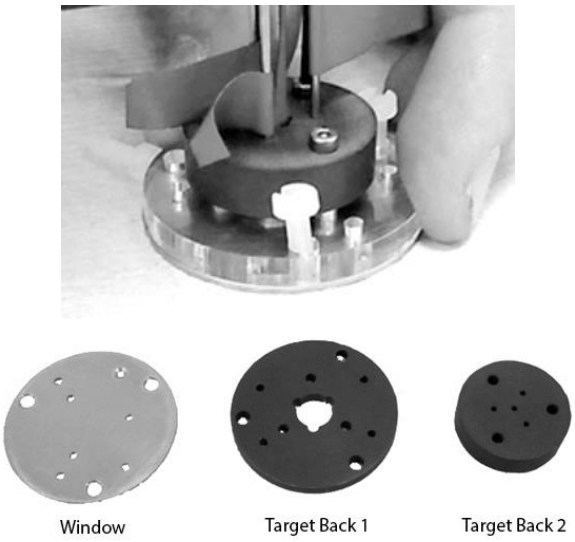

Figure 3.3. Target and its respective components.

There are 4 probes that in this work are denominated from A to D, whose positions are represented in Figure 3.4.

The probe A is in the back of the sample and the probes B, C and D are surrounding the sample measuring the free surface velocity history of the window. They are spaced 120° in order to accurately determine a possible tilt in the propagation of the shock wave. When everything in place the target was attached with nylon screws to the adjustable mount in the target chamber at the end of the barrel. During setup the mount was adjusted such that the target was perfectly planar to the flyer. This was accomplished using laser alignment techniques.

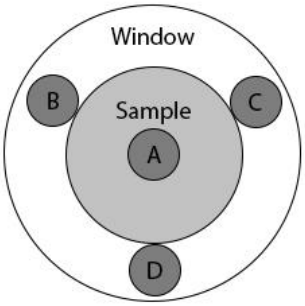

Figure 3.4. Probes position.

For the shot, the target chamber was sealed with everything into position. The expansion tank attached to the target chamber is to allow the gas to expand. The breach, target chamber and expansion tank were placed under vacuum. Meanwhile, the gas tanks are pressurised with helium to a determined pressure to produce the desirable projectile velocity. When the launcher was "fired" the expansion of the gas pushes the projectile through the barrel until it reaches the target with its maximum velocity.

3.2.1. Alignment

To centre the adjustable mount with the barrel it was used a rod that fits tight into the barrel and in the adjustable mount. Its alignment with the barrel was done with an accuracy better than 1/10 mm.

The adjustable mount tilt was adjusted in two stages with the use of a laser as shown in Figure 3.5. The first stage (top image) a laser on the left side was centred with the 3 meter long barrel and then used to align the two irises I1 and I2 that are 200 mm apart from one another. In the last stage (bottom image) a mirror M was placed on the right face of the target holder to reflect a laser centred with the irises. The tilt was adjusted by observing the laser reflection on the left side of the irises. The adjustable mount tilt was adjusted with an accuracy better than 3 mrad.

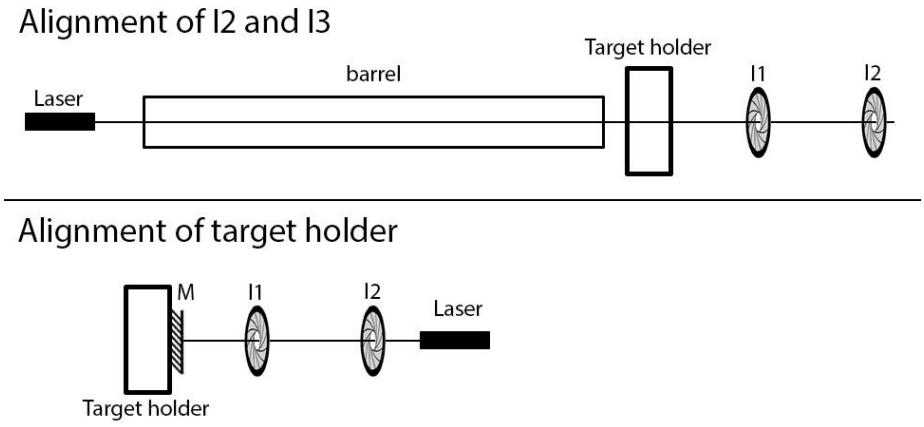

Figure 3.5. Target holder alignment.

3.3. Plate Impact specimen geometry

Three samples of the B_4C-7at.%Si system were studied in plate impact experiments.

As was mentioned before, the ceramic mixture was prepared previously by others colleagues from DEM-UC [8,9]. The ceramic samples were constrained within frames of steel, that serves as support for the sample until is subjected to the impact, with diameter d_s and thickness e_s, as can be seen in Figure 3.6. For that, a special die was prepared, Figure 3.7.Die and its respective componentsFigure 3.7, the 2D technical drawings are in the Annex A.

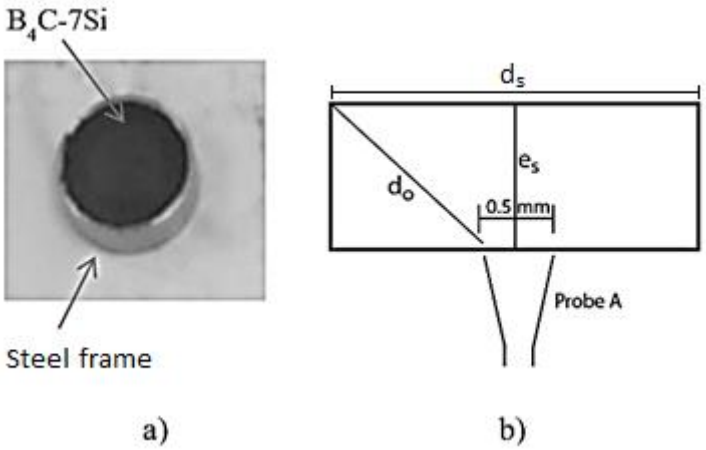

Figure 3.6. a) Optical image of a sample; b) Shock wave paths in the sample.

Figure 3.7. Die and its respective components.

The sample diameter d_s was determined to be of 7.5×10^{-3} m it was limited by the impactor's size of 12.5 mm, the space needed for the probes B, C and D surrounding the sample and for the steel frame.

It is necessary to have 1-D configuration in the back of the sample without release waves from the outer surfaces during a sufficient period of time, t_w, to gather the necessary data. The free surface of the sample needs to reach its maximum velocity and be analysed for a brief period of time in order to determine the particle velocity. From the literature results analyse it was selected that a time frame of 4.5×10^{-7} s is sufficient.

The equation to calculate the maximum thickness for the sample, e_s, to assure the 1-D configuration for the time frame stipulated can be deduced geometrically from Figure 3.6 b) by comparing the times that the plane shock wave, t_{e_s}, and the outer surface shock wave, t_{d_o} takes to reach the measuring zone of the probe is given by:

$$t_w = t_{d_o} - t_{e_s} = \frac{\sqrt{\left(\frac{d_s - 5 \times 10^{-4}}{2}\right)^2 + {e_s}^2}}{U_{s_{sample}}} - \frac{e_s}{U_{s_{sample}}} \tag{3.1}$$

Where,

d_0 and e_s - the shorter paths for an outer surface and a plane shock waves to reach the measuring zone of the probe, respectively,

e_s - correspond to the sample's thickness

$U_{s_{sample}}$ - premeditated maximum shock wave velocity for the experiments, with a value of 5000 m/s.

$$4.5 \times 10^{-7} = \frac{\sqrt{\left(\frac{7.5 \times 10^{-3} - 5 \times 10^{-4}}{2}\right)^2 + {e_s}^2}}{5000} - \frac{e_s}{5000} \tag{3.2}$$

$$e_s = 1.6 \times 10^{-3} \text{ m}, \tag{3.3}$$

Thus, the maximum thickness value for the ceramic sample is 1.6 mm.

A brass layer, with 25 μm of thickness, was placed in the back of the sample for better reflexion of the probe's light.

The samples were pressed into discs with approximately 1 mm thickness constrained within frames of steel that serves as support for the sample until is subjected to the impact.

3.4. HetV

The data was collected using HetV with probes focused on the back surface of the specimen and window. The light was produced by an infrared laser operating at 1550 nm and transported by all-glass single-mode fibers, standard in the telecommunications industry. A Lecroy WaveMaster 816Zi-B Oscilloscope with a bandwidth of 16GHz and sampling rate up to $40GS/s$ was used to collect the experimental data. The sampling rate used in the experiment was of 20GS/s with intervals of 50 ps. A labview program interface was used for operating the gun and a matlab program was used to analyse the HetV data. The matlab program converted interference fringes to free surface velocities.

For the probes, bare fibers with the configuration shown in Figure 3.8, was used.

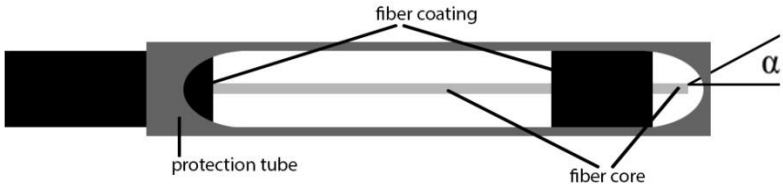

Figure 3.8. Probe schematic used in this work.

The cables were all cut with the same length, 800 mm, with an accuracy of 0.5 mm. The cable point was stripped and cut with a high precision cleaver. A 50 mm long tube was glued in the cable point to straight up and protect the end face of the fiber. The gap without coating inside the tube is to allow the fiber to be as straighten as possible close to its end. The numerical aperture NA of the probe was 0.22. The probes were placed to a distance of less than 1 mm from the surfaces.

4. RESULTS AND DISCUSSION

As was mentioned before, three plate impact experiments in the velocities range from 300 to 700 m/s were done. The main samples characteristics are summarized in Table 4.1

Table 4.1. Main characteristics of the B_4C-7at.Si samples.

Sample	Thickness, e_s (mm)	Mass, m (g)	Density, ρ_0 (Kg/m^3)	Impact Velocity, V (m/s)
#01	0.836	0.0558	1.512	314
#02	0.836	0.0577	1.561	495
#03	0.947	0.0644	1.539	690

It is important to mention that the small scale, using a 13 mm bore single-stage meso-scale launcher was used for the first time.

It was also necessary to design and manufacture a target to hold the sample and the probes used in the front of the launcher. A special die to compact the sample was also built. These processes took some time; especially the manufacture of the die and the target that first was sent to the ICL´s workshop and due to delays was finally manufactured in the DEM´s workshop at UC and sent to London. All the experiment was done in an optimization phase.

As can be concluded by the analysis of Table 4.1, the thickness of all the samples are less than the maximum value previewed ($e_s = 1.6 \times 10^{-3}$ m, equation (3.1)).

The respective density, ~ 1.5 Kg/m^3, gives rise to 60% TMD. This was obtained assuming the B_4C-7Si bulk density similar to the bulk density of the B_4C (2.52 Kg/m^3 [8]). The density calculations were done by comparing the volume determined by the measurement of its thickness Δx with the mass m of the sample with accuracies of 0.1 mm^3 and 0.1 mg, respectively.

Before testing the B_4C-Si samples, it was necessary to do an experiment on a target without sample in order to calibrate the detector and the digitizer channels.

4.1. HetV Calibration

The probes of each experiment are connected to four different channels of the detector to be converted into analogic signals and then analysed by the oscilloscope. Each channel was a slightly different time response due to their components. In order to compare the four signals in each experiment it is necessary to determine the difference of the time responses of the channels and correct it in the results. The time correction can be determined by giving the same signal to all the channels and compare the results. For that it was done a plate impact experiment with only one probe measuring the free surface of a copper plate. The probe was connected to a 1×4 fiber splitter to divide the signal into four equal signals. The resultant response of the four signals in the digitizer is shown in Figure 4.1.

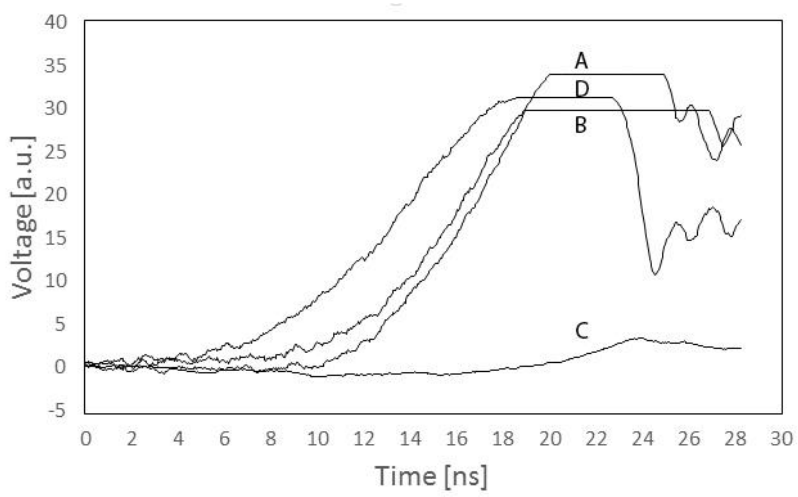

Figure 4.1. Moving average trend line of the four signals from each channel in the calibration experiment.

It was determined the correction times of the channels by adjusting the curves of channels B, C and D having the curve of the channel A as a reference. The adjusted curves and the resultant time corrections are shown in Figure 4.2, resulting from the following approach:

A = + 0.0 ns (reference) B = + 1.0 ns

C = - 7.0 ns D = +6.0 ns

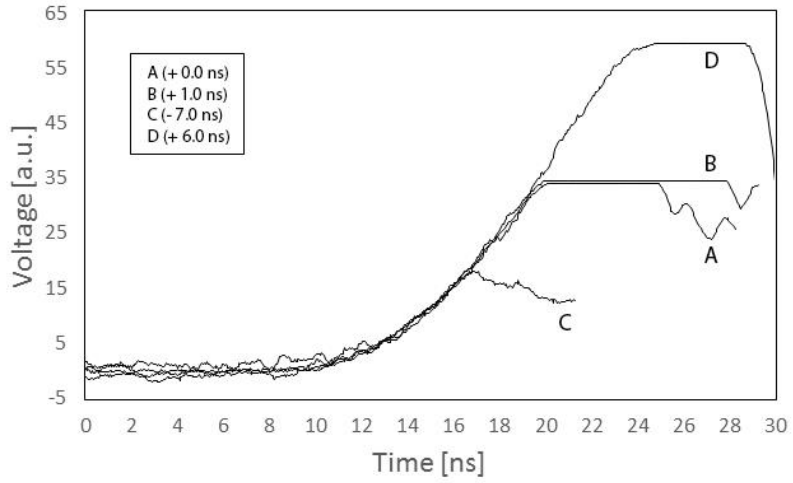

Figure 4.2. Time correction of the channels.

4.2. Shock Wave Velocity (U_s)

The shock wave velocity, U_s, was determined by the velocity equation knowing the time that the shock wave takes to pass through the sample, Δt, and its thickness, e_s.

When a shock wave arrives to a free surface that surface immediately starts to move. To determine the arrival time of the shock wave t_i it was observed the free surface of the copper plate that is immediately before the sample and assumed that the arrival time of the shock wave to that surface correspond to the arrival time of the shock wave to the sample.

The free surface of the copper has three probes B, C and D to measure its response in order to determine the tilt of the shock wave when it reaches the sample and, therefore, the accuracy of the resultant shock wave velocity. The probe A placed in the back of the sample will determine the arrival time of the shock wave t_f.

The resultant data from the HetV analyse is expressed into a beat amplitude in function of time. When the measured surface start to move its velocity is directly translated in the beat signal as a frequency. Therefore, analysing the data it is possible to locate the time when the beat signal response has some frequency associated.

In the Figure 4.3 to Figure 4.5 are shown the resulting beat waveform as a function of time of each experiment with the corresponding arrival times of the shock wave, for the tree samples.

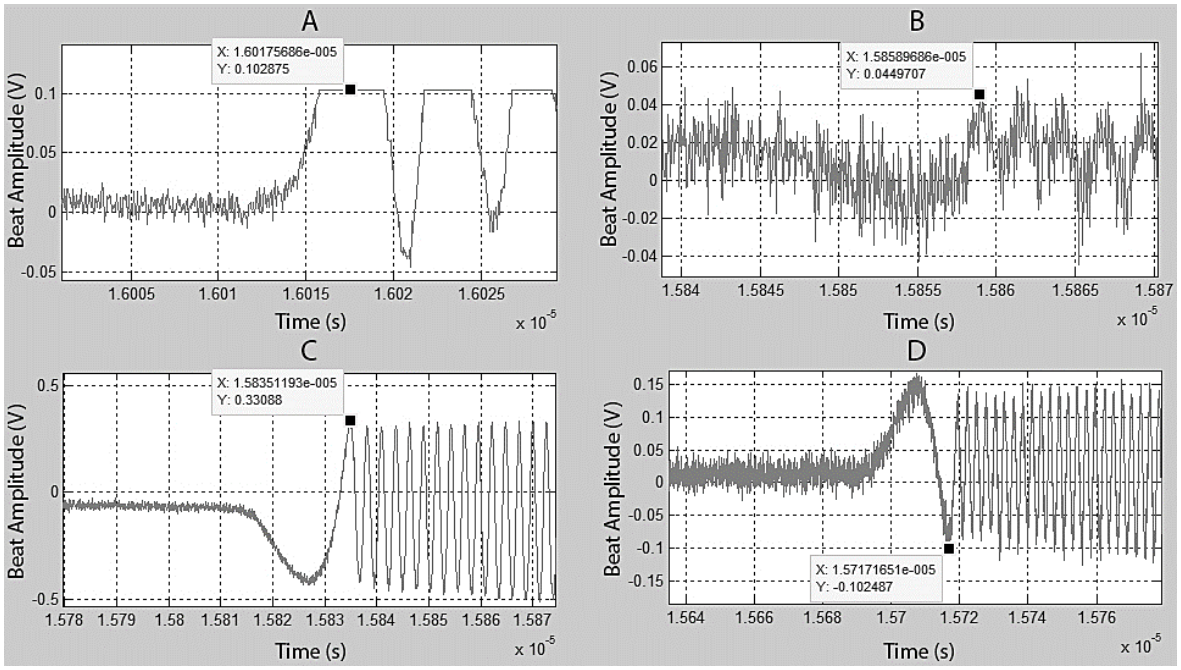

Figure 4.3. Plot signal from the plate impact experiment on Sample #01.

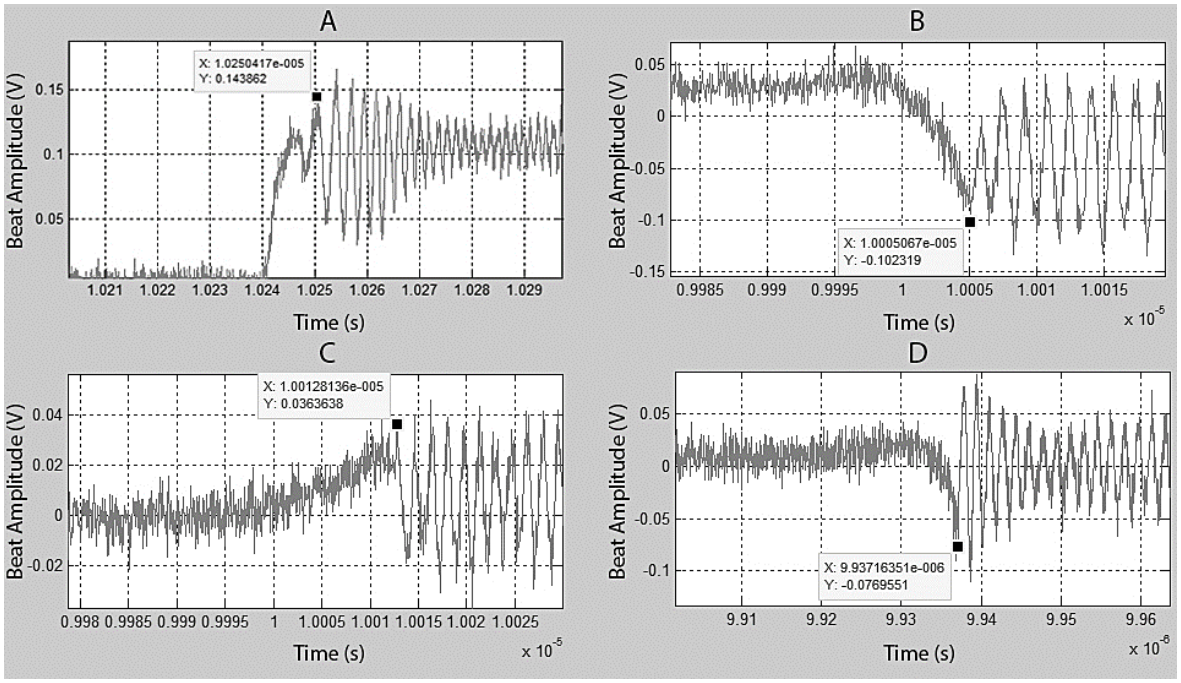

Figure 4.4. Plot signal from the plate impact experiment on Sample #02.

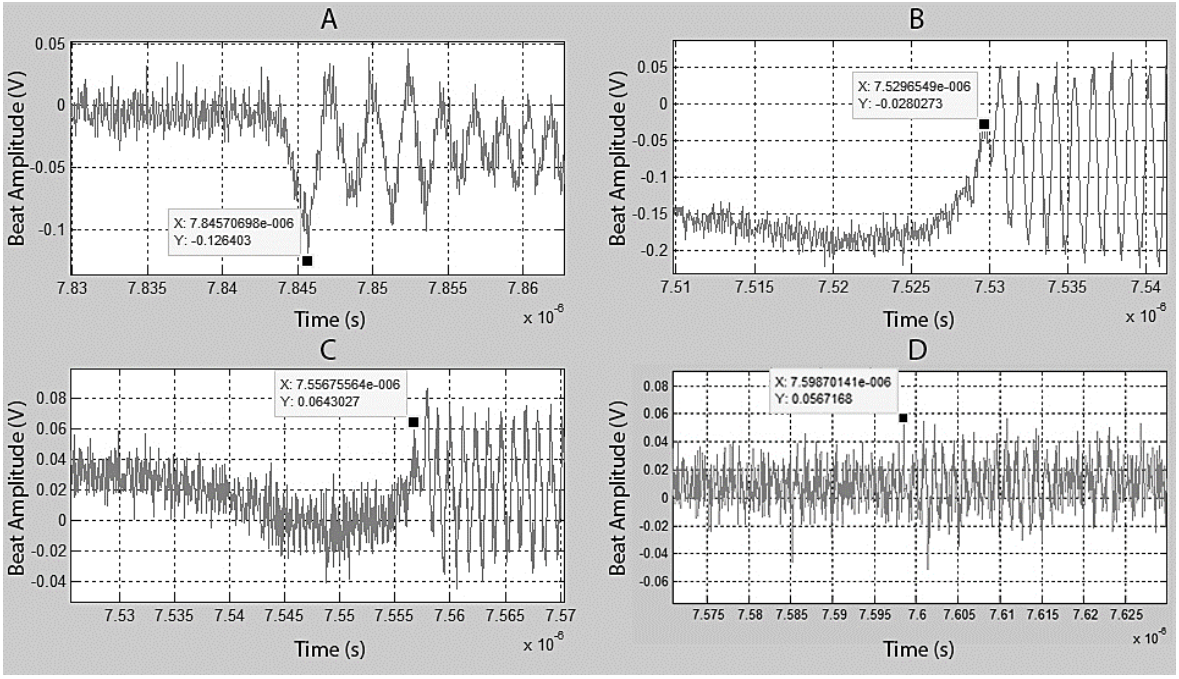

Figure 4.5. Plot signal from the plate impact experiment on Sample #03.

In the plate impact experiment on the sample #01 the signal from the probe A has a flat line with 0.1 V corresponding to a saturation of the probe. Nevertheless is still evidently the start of frequency in the beat signal. The signal B has lower amplitude so it takes a more careful look to identify the arrival time of the shock wave. The arrival of the shock wave in the probes C and D are perfectly clear.

For the experiment on the sample #02 in comparison with #01 the arrival times of the shock waves are very clear for all four signals, as can be seen in Figure 4.4.

Considering the last sample, #03 (Figure 4.5) it is very difficult to identify the time of arrival of the shock wave in probe D. Nevertheless, by a carefully analysis, it is possible to identify some frequency after 7.6×10^{-6} s. All the other probes have clear signals and are easy to identify its shock waves arrival times.

The arrival times of the shock waves in each probe, which includes the corrections from the HetV calibration (Figure 4.2), are summarized in Table 4.2.

Table 4.2. Shock waves arrival times (accuracy better than 5 ns).

Sample	A (ns)	B (ns)	C (ns)	D (ns)
#01	16018	15860	15828	15723
#02	10250	10006	10006	9943
#03	7846	7531	7550	7599

Based on shock waves arrival times data, Table 4.2, the respective shock wave velocity, Us, for each sample, was calculated. The results obtained are summarized in Table 4.3. The shock waves arrival times to the sample t_i was assumed to be the average of arrival times of the shock waves to the probes B, C and D. The time that the shock wave takes to go through the sample, Δt was determined by the difference between t_i and t_f.

Table 4.3. Shock Wave velocity.

Sample	t_i (ns)	t_f (ns)	Δt (ns)	e_s (mm)	U_s (m/s)
#01	15804	16018	214	0.836	3900
#02	9985	10250	265	0.836	3155
#03	7560	7846	286	0.947	3311

The shock wave time of the sample #01 is much greater than the shock waves velocities from the samples #02 and #03. This behaviour can be related to some error resulting from the great tilt observed in the first experiment associated to the difference in the times of the probes B to D with a maximum absolute value of 137 ns on the sample #01compared to the 63 and 68 ns for the samples #02 and #03.

4.3. Particle Velocity (u_p)

The particle velocity, u_p, was determined by data analyse of the free surface velocity history. The free surface has velocity of twice the particle velocity, as can be concluded by analysing the Figure 2.7.

In the Figure 4.6 to Figure 4.8 the free surface velocity as a function of time of the three experiments resultant from the sliding fast Fourier transform applied to the beat signal are represented. The sliding fast Fourier transform was performed in 512 points (window size) and with an overlap of 80% of the window size. The particle velocity of each experiment was assumed to be the average of the velocities after the velocity profile stabilizes.

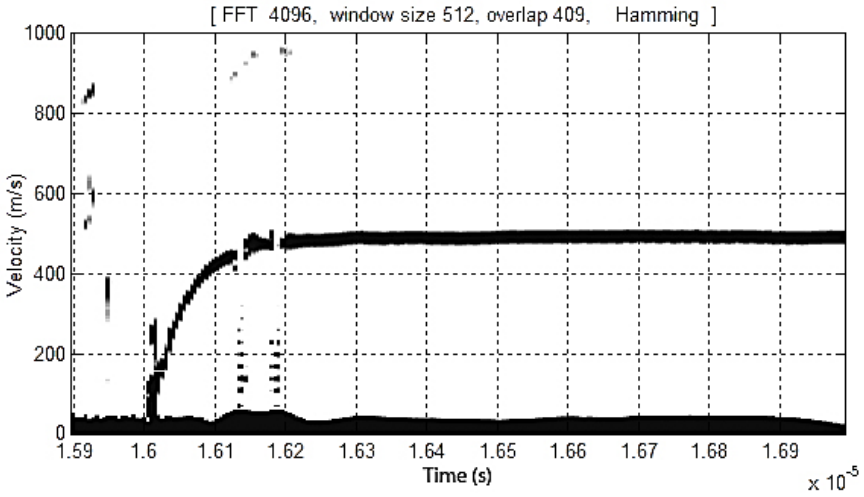

Figure 4.6. Free surface velocity profile of Sample #01.

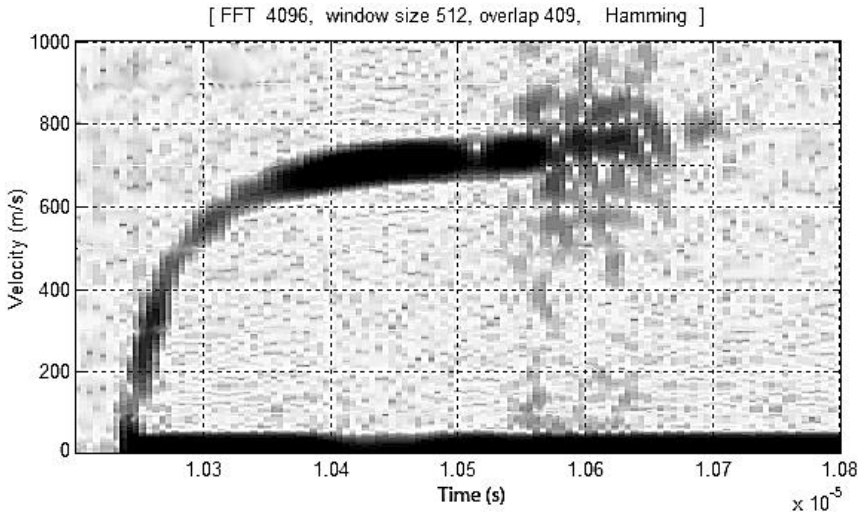

Figure 4.7. Free surface velocity profile of Sample #02.

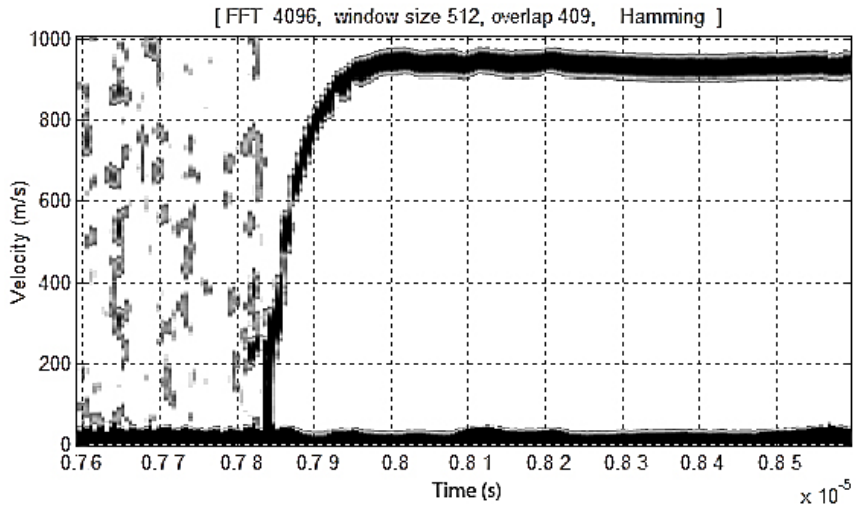

Figure 4.8. Free surface velocity profile of Sample #03.

The free surface of the sample #01 stabilized its velocity around 1.63×10^{-5} s, as can be seen in Figure 4.6. The free surface maintains its velocity for 700 ns, which was the interval chosen to calculate the particle velocity. In that interval the average velocity of the free surface was of 490 m/s corresponding to a particle velocity for the sample #01 of 245 m/s.

For the sample #02, the interval of time selected to calculate the particle velocity was between 1.04×10^{-5} s and 1.05×10^{-5} s, thus the average velocity of the free surface is 708 m/s and the particle velocity is 354 m/s.

Finally, the sample #03 presents a stabilized free surface velocity for the interval of time between 0.80×10^{-5} s and 0.85×10^{-5} s, Figure 4.8. For this sample the velocity of the free surface was 938 m/s and the respective particle velocity was 469 m/s.

The particle velocities for the B4C-7Si system are summarized in Table 4.4.

Table 4.4. Experimental data.

Sample	Impact Velocity, V (m/s)	Shock Wave Velocity, U_s (m/s)	Particle Velocity, u_p (m/s)
#01	313	3900	245
#02	493	3155	354
#03	688	3311	469

By analysing the results from the experiments, Table 4.4, one can conclude that the impact velocity in each experiments increases and the respective particle velocity had the same behaviour, as was expected. However, the same cannot be said for the shock velocity. In fact, the value for the sample #01 is much higher in comparison to the other two experiments. This behaviour, as was referred before, could be attributed to the great tilt of the impactor leading to a tilt in the shock wave itself.

4.4. Hugoniot Parameters

The experimental Hugoniot parameters were determined from a linear regression in the U_s-u_p plane, using the equation (2.10), that is:

$$U_s = C_0 + Su_p,$$

The B_4C-7Si Hugoniot system, for 60% TMD, is presented in Figure 4.9, for U_s-u_p plane. Although the results from the experiment #01 be presented, it were not taken into account in linear regression.

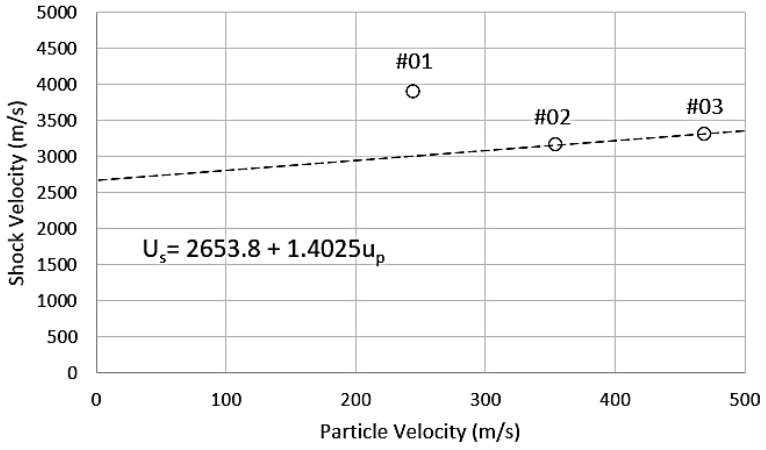

Figure 4.9. Experimental results in the U_s-u_p plane with linear regression of the results of the samples #02 and #03.

The linear Hugoniot slope coefficient for the material in study is 1.4025. This value match the S literature value, typically approximately 1.5 [29].The B_4C-7Si bulk sound speed present a value of 2653.8 m/s.

The experimental results in the plane p-ν can be seen in Figure 4.10. The initial specific volume, ν_o, of 0.65 cm^3/g at zero pressure is also presented.

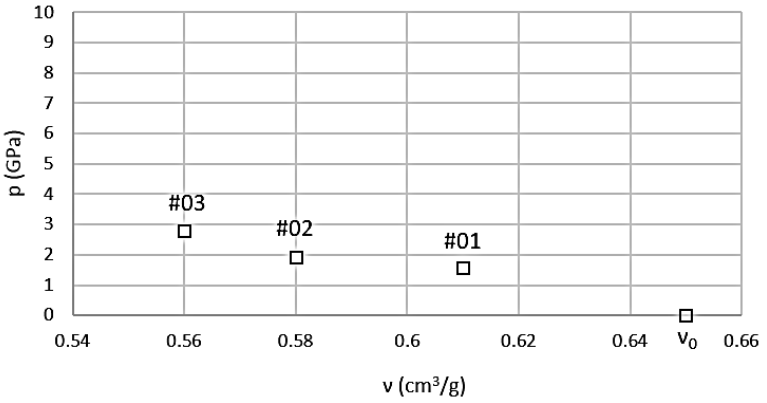

Figure 4.10. Experimental results and the initial density in the p-ν plane.

In order to conclude if the addition of 7at % Si to B_4C by Mechanical Alloy increases or not the ballistic properties, it is important to compare these experimental results with those obtained by other research workers, mainly those obtained by Grady [12] in Figure 4.11.

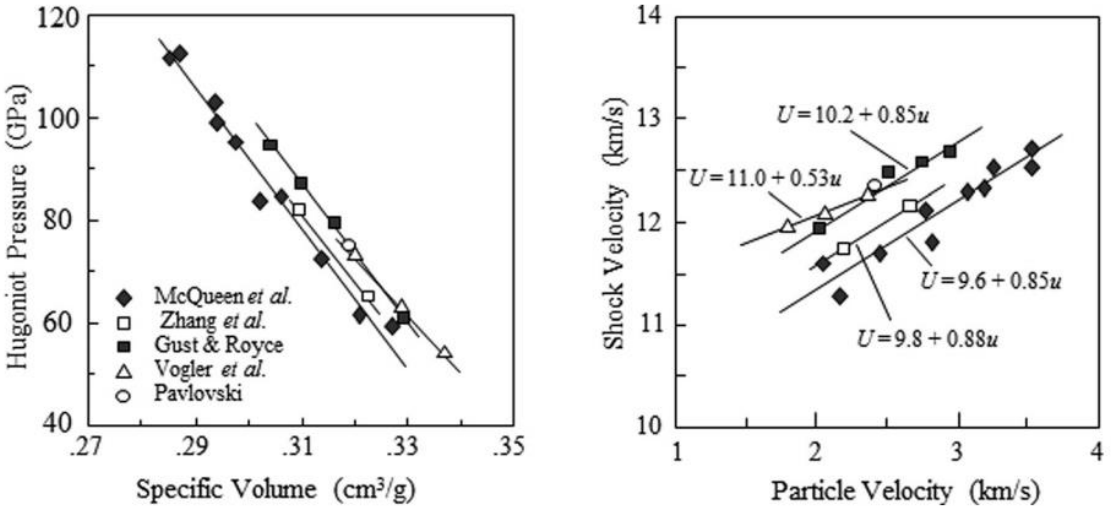

Figure 4.11. Comparisons of solid boron carbide Hugoniot data **[12]**.

However, such relationship is very difficult to achieve since the actual experiments reach pressures below 3 GPa, while the available data for B_4C is between 50

and 120 GPa. In fact, in the present work the impact velocities range from 300 to 700 m/s. Moreover, the B_4C-7Si could not be considered a bulk material due to its 60% TMD. Thus, the ceramic system was addressed as porous material. Several models to forecast this behaviour were used.

4.5. Theoretical Approach

As was mentioned before (Chapter 2), there are two models for the determination of the Hugoniot of porous materials: the Thouvenin and Gruneisen models.

Thus, for the Gruneisen model, the pressure in function of the specific density was calculated applying for equation (2.24). The shock and the particle velocities were obtained from the pressure by rearranging the equations (2.3) and (2.6). Aimed the Plate Gap Model, usually denoted as Thouvenien, the equations (2.25) and (2.26) were employed for the determination of the shock and particle velocities; while the pressure and the specific density evaluation were done by using equations (2.3) and (2.6).

The theoretical approach obtained could be seen in Figure 4.12 for both planes, U_s-u_p and p-ν.

It is important to refer a first approximation in the construction of the models, the parameters of Hugoniot and Gruneisen of the solid B_4C-7at.%Si system were assumed to be the same as the parameters of the solid B_4C since the percentage of Si in the material is very small.

The same was done for the initial density of the solid material. The parameters of the B_4C were determined from Marsh´s work [30]. The initial density of the porous material was calculated to be the average of the densities determined for the three samples.

Considering the evolutions shown in Figure 4.12, the sample #01, as expected, is farther from both models. This confirms the previous results, assigned to the large tilt experiment. Reflecting #02 and #03 samples, both form a similar slope as the models. Although, mutually have a shock wave velocity higher than expected from the models.

A possible explanation for these deviations may be related with the low pressures used experimentally in this work (less than 5GPa) in opposite with the models, which were verified to be reliable for higher pressures (25-160 GPa).

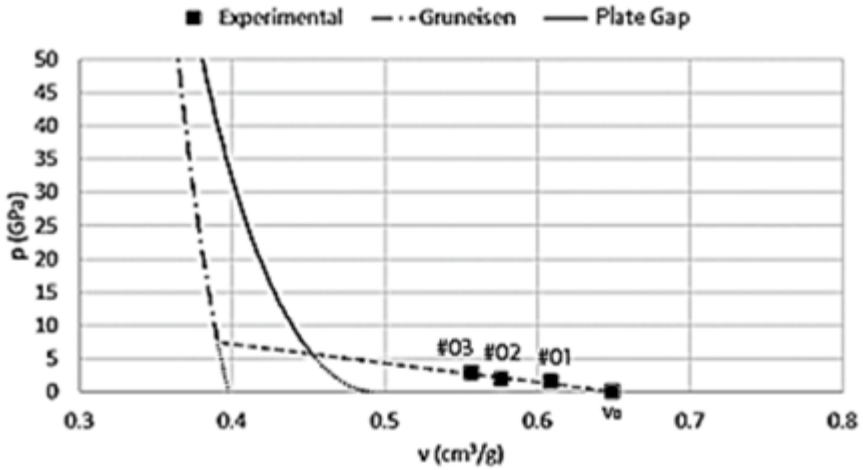

Figure 4.12. Representation of the experimental data and the models of Gruneisen and Thouvenin for porous materials in the p-v plane.

Another attempt was made to compare the results obtained at IPS with those available in the literature. The Marsh [30] results were selected.

Figure 4.13, show the results concerning porous B_4C material with 95%TMD and 75%TMD obtained by Marsh, which were overlapped with those obtained in the present work.

Considering the U_s-u_p plane, the three experiments look that they are aligned with the results of the low TMD B_4C but with much lower shock and particle velocities

However, for the p-v plane the analyse is more ambiguous due to the very low pressures obtained but focusing in the result for the initial density, with zero pressure, of the three different densities the results on B_4C-7Si system follow the tendency.

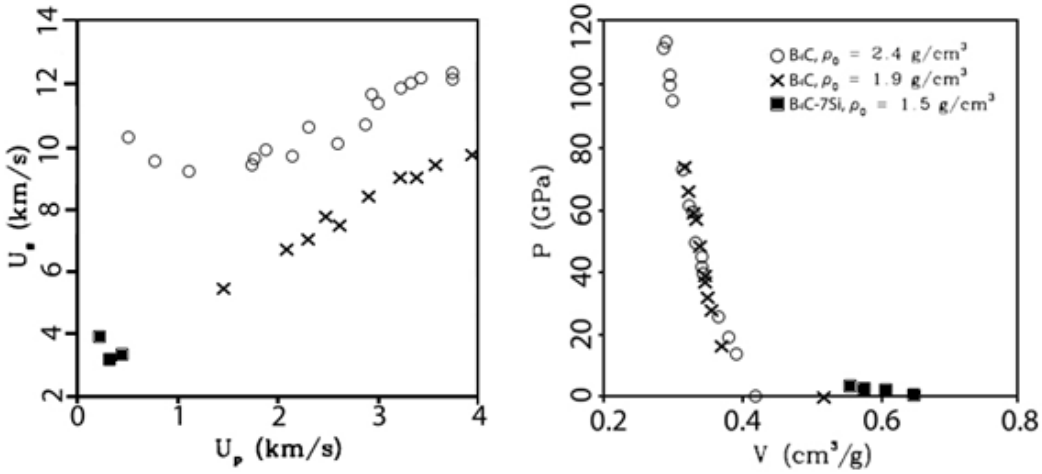

Figure 4.13. Hugoniot results on porous B_4C from Marsh **[30]** with different initial densities comparisons with results from this report.

5. CONCLUSIONS AND SUGESTIONS

This report summarizes the stages for the realization of plate impact experiments for the determination of the Hugoniot parameters of the ceramic B_4C-7Si system using a gas gun. The experiments were performed at projectile velocities of 313, 493 and 688 m/s obtaining pressures in the range of 1.5 to 2.8 GPa. This stress created a shock with velocities of approximately 866 to 1620 m/s which imparted particle velocities between 151 and 300 m/s.

The principal conclusions of the thesis are:

-The design of a die to press small and thin samples of powder to be used in plate impact experiments was done. Also the design of a target for plate impact experiments with small bore, 10 mm to 15 mm bore high velocity projectile launchers.

-It was observed a significant tilt in the impactor at the moment of impact which originated some errors in the results of the shock velocity.

-The parameters of Hugoniot can only be used as a reference for a first approximation and not as the exact values because it was done few impact experiments and the range of pressures covered by the experiments is small.

-The theoretical predictions for porous materials were also investigated in this study. However, the results showed that the theoretical calculations are not in good agreement with the experimental data and the results obtained are in general lower than the predict values. Two possible reasons are pointed out. The approximation done by using the parameters for the solid boron carbide or the material may not have been fully compacted for impact of lower velocities.

-The experimental results follow the same tendency as the ones for porous boron carbide from Marsh [30].

For future works it is suggested a comparison of the Hugoniot relation of solid B_4C and B_4C-7Si system at higher velocities, as well a comparison with Hugoniot relation for pure B_4C in the same experimental conditions.

6. REFERENCES

[1] Teixeira-Dias, F., Dodd, B. & Coghe, F. (Eds.) (2011). *New Design Concepts in Light-Weight Armour for Vehicles*. (1 ed.) LWAG - Light-Weight Armour for Defence and Security.

[2] Wilkins, M., Honodel, C. & Swale, D. (1967, June). *An Approach to the Study of Light Armour*. Lawrence Radiation Laboratory, Livermore, UCRL-50284.

[3] Wilkins, M., Landingham, R. & Honodel, C. (1971, January). *Fifth Progress Report of Light Armour Program*. Lawrence Radiation Laboratory, Livermore, UCRL-50980.

[4] Wandley, H. N. G., O'Masta, M. R., Dharmasena, K. P., Compton, B. G., Gamble, E. A. & Zok, F. W. (2013, December). Effect of core topology on projectile penetration in hybrid aluminum/alumina sandwich structures. *International Journal of Impact Engineering, 62*, 109-113.

[5] Thévenot, F. (1990). Boron Carbide - A Comprehensive Review. *Journal of the European Ceramic Society, 6,* 205-225.

[6] Dandekar, D. P. (2001. April). *Shock Response of Boron Carbide*. ARL-TR-2456, Army Research Laboratory.

[7] Fanchini, G. & Chhowalla, M. (2006). On ballistic performances of boron carbide. *Materials science and engineering - Rugtger university - 08854 Piscataway, NJ(USA).*

[8] Costa, A. R. C. F. (2011, September). *Consolidação dinâmica de cerâmicos leves à base de B4C*. Master Thesis in Mechanical Engineering - University of Coimbra, Coimbra.

[9] Frade, J. F. C. (2012, June). *Compactação Dinâmica de Materiais Cerâmicos para Protecção Balística*. Master Thesis in Mechanical Engineering - University of Coimbra, Coimbra.

[10] Grady, D. E. (1998, August). Shock-wave compression of brittle solids. *Mechanics of Materials, 29(3-4),* 181-203.

[11] Grady, D. E. (1994, September). Shock-wave strength properties of boron carbide and silicon carbide. *Journal de Physique IV, 04(C8),* 385-391.

[12] Grady, D. E. (2015). Hugoniot equation of state and dynamic strength of boron carbide. *Journal of Applied Physics, 117.*

[13] Grady, D. E. (1995). *Dynamic Properties of Ceramic Materials.* SAND 94-3266, Sandia National Laboratories.

[14] Wilkins, M. L. (1968). *Third Progress Report of Light Armor Program.* Lawrence Livermore National Laboratory, University of California, CA.

[15] Gust, W. H. & Royce, E. B. (1971). Dynamic Yield Strenghts of B4C, BeO and Al2O3 Ceramics. *Journal of Applied Physics, 42*, 276-295.

[16] Pavlovskii, M. P. (1971). Shock Compressibility of Six Very Hard Substances. *Soviet Physics-Solid State, 12*, 1737.

[17] Vogler, T. J., Reinhart W. D. & Chhabildas, L. C. (2004). Dynamic behavior of boron carbide. *Journal of Applied Physics, 95*, 4173-4183.

[18] Rajendran, A. M. & Grove, D. J. (1996). Modeling the shock response of silicon carbide, boron carbide and titanium diboride. *International Journal of Impact Engineering 18,* 611.

[19] Chen, M. W., McCauley, J. W. & Hemker, K. J. (2003). Shock-induced localized amorphization in boron carbide. *Science, 299,* 1563.

[20] Rosenberg, Z. & Yeshurun, Y. (1985). Determination of the dynamic response of AD-85 alumina with in-material gauges. *Journal of Applied Physics, 58*, 3077.

[21] Louro, L. H. & Meyers, M. A. (1989). Effect of stress state and microstructural parameters on impact damage of alumina-based ceramics. *Journal of Materials Science, 24,* 2516.

[22] Bartkowski, P. T., Dandekar, D. P. & Grove, D. J. (2001). *Spallation of Hot Pressed Boron Carbide Ceramic*. Army Research Laboratory.

[23] Winter, R. (2009, December) *Key Concepts of Shock Hydrodynamics.*

[24] Zhang, Y., Mashimo, T., Uemura, Y., Uchino, M., Kodama, M., Shibata, K., Fukuoka, K., Kikuchi, M., Kobayashi, T. & Sekine, T. (2006). Shock compression behaviors of boron carbide (B4C). *Journal of Applied Physics, 100(11)*.

[25] Thouvenin, J. (1965). Effect of a shock wave on a porous solid. *Fourth International Symposium on Detonation.* Office of Naval Research, Department of the Navy, Washington DC, EUA. 258-265.

[26] Hofmann, R., Andrews, D. & Maxwell, D. (1968). Computed shock response of porous aluminium. *Journal of Applied Physics, 39*, 4555-4562.

[27] Barker, L. M. & Hollenbach, R. E. (1972, April). Laser interferometer for measuring high velocities of any reflecting surface. *Journal of Applied Physics, 43.*

[28] Strand, O. T., Berzins, L. V., Goosman, D. R., Kuhlow, W. W., Sargis, P. D. & Whitworth, T. L. (2014, August). *Velocimetry using heterodyne*. UCRL-CONF-206034, Alexandria, VA, United States.

[29] Hayes, D. B. (1973, August). *Introduction to stress wave phenomena*.

[30] Marsh, S. P. (1980). *LASL Shock Hugoniot Data*. Los Alamos Series on Dynamic Material Properties.

[31] Winter, R. (2009). *Shock compression behaviors of boron carbide*.

[32] Ribeiro, J. M. B. M. S. (2003). *Propagação de ondas de choque em espumas sintácticas.* Departamento de Engenharia Mecânica, Faculdade de Ciências e Tecnologia, Universidade de Coimbra, Coimbra.

[33] Nuttall, A. H. (1971). *Spectral Estimation by Means of Overlapped Fast Fourier Transform Processing of Windowed Data.* Naval underwater systems center.

[34] McQueen, R. G., Marsh, S. P., Tayler, J. W., Fritz, J. N. & Carter, W. J. (1970). The equation of state of solids from shock wave studies. *High Velocity Impact Phenomena*, New York, 293-417;521-568.

[35] Holmquist, T. J. & Johnson, G. R. (2006). Characterization and evaluation of boron carbide for plate-impact conditions. *Journal of Applied Physics, 100*.

[36] Heyda, J. F. (1968) *Plate-Gap model of a porous solid and its application to impact by reduced density projectiles*. National aeronautics and space admnistration, Washington, D. C..

[37] Carton, E. P. (1998). *Shock Compaction of Ceramics and Composites.* Delft University Press.

[38] Zel'Dovich, Y. & Raizer, Y. (1967). *Physics of shock-waves and high-temperature hydrodynamic phenomena*. Academic Press Inc., New York.

ANNEX A

The 2-D drawings of the die are presented in the following pages. The die is to uniaxially press a powder material into a sample of 7.5mm diameter and thickness from 0.5 mm to 3 mm contained within a steel frame of 0.5 mm wall thickness.

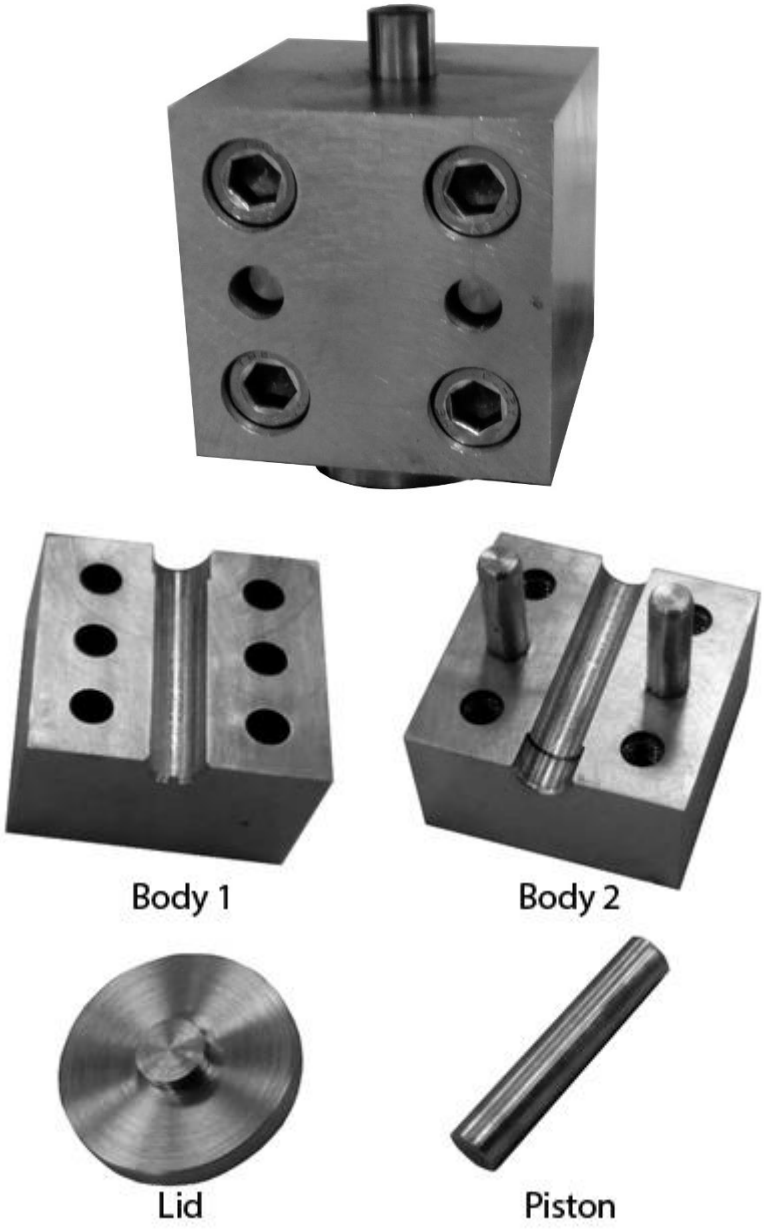

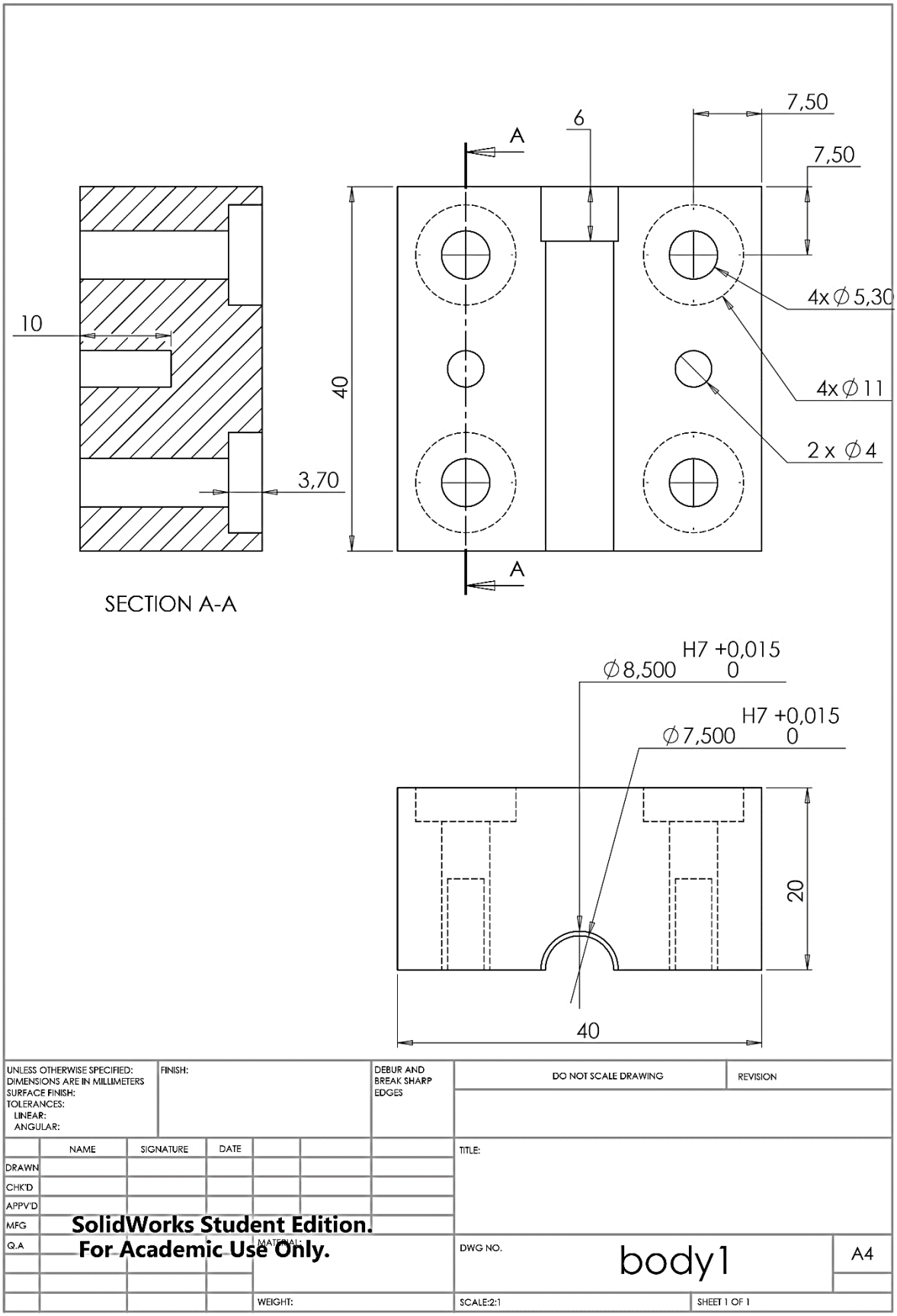
7,50
6
A
7,50
4x ∅ 5,30
10
40
4x ∅ 11
2 x ∅ 4
3,70
A
SECTION A-A
H7 +0,015
∅ 8,500 0
H7 +0,015
∅ 7,500 0
20
40
UNLESS OTHERWISE SPECIFIED:
DIMENSIONS ARE IN MILLIMETERS
SURFACE FINISH:
TOLERANCES:
LINEAR:
ANGULAR:
FINISH:
DEBUR AND BREAK SHARP EDGES
DO NOT SCALE DRAWING
REVISION
NAME
SIGNATURE
DATE
DRAWN
CHK'D
APPV'D
MFG
Q.A
TITLE:
SolidWorks Student Edition.
For Academic Use Only.
MATERIAL:
DWG NO.
body1
A4
WEIGHT:
SCALE:2:1
SHEET 1 OF 1

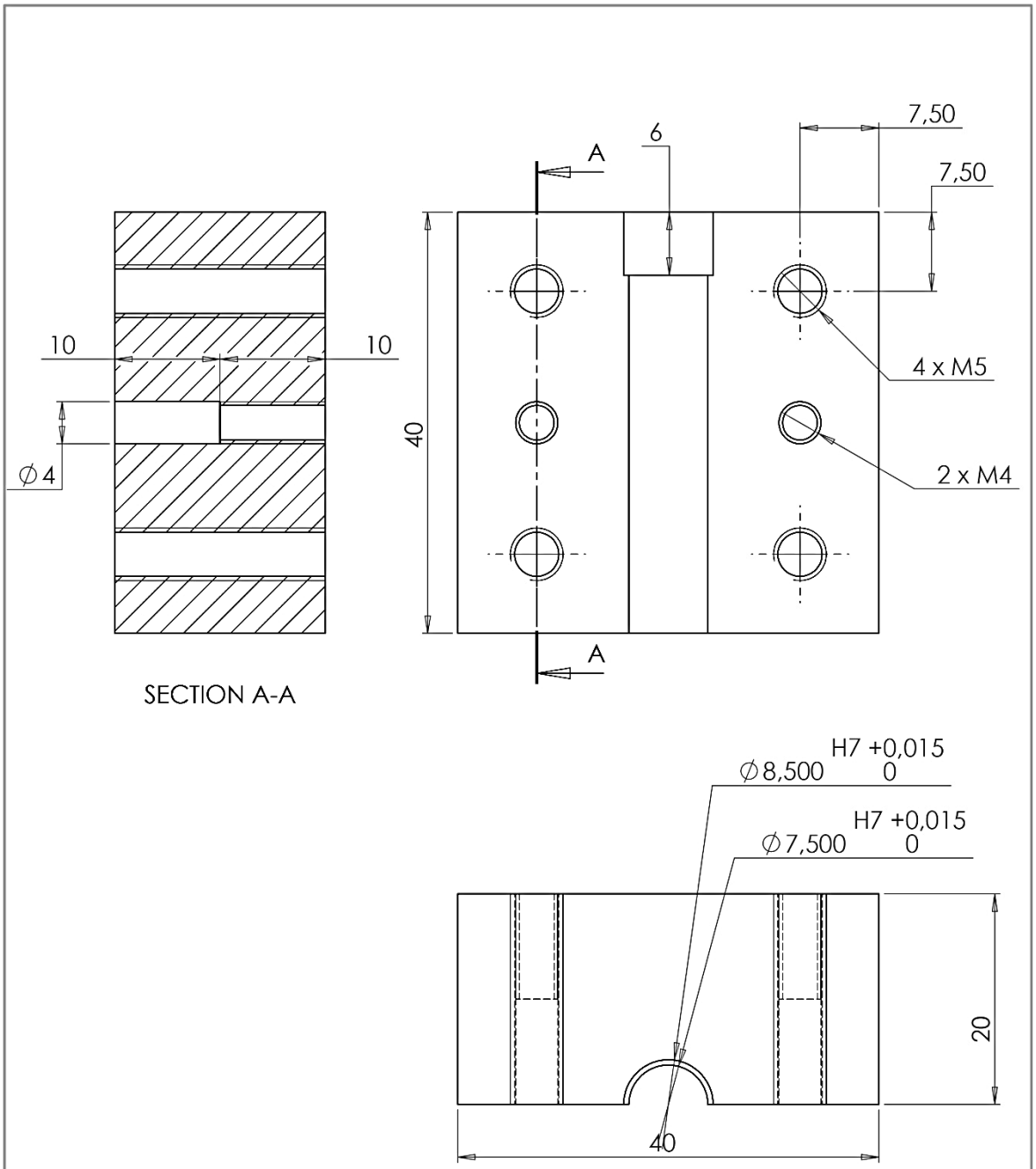

UNLESS OTHERWISE SPECIFIED: DIMENSIONS ARE IN MILLIMETERS SURFACE FINISH: TOLERANCES: LINEAR: ANGULAR:		FINISH:			DEBUR AND BREAK SHARP EDGES	DO NOT SCALE DRAWING	REVISION
	NAME	SIGNATURE	DATE			TITLE:	
DRAWN							
CHK'D							
APPV'D							
MFG							
Q.A				MATERIAL:		DWG NO. body2	A4
				WEIGHT:		SCALE:2:1	SHEET 1 OF 1

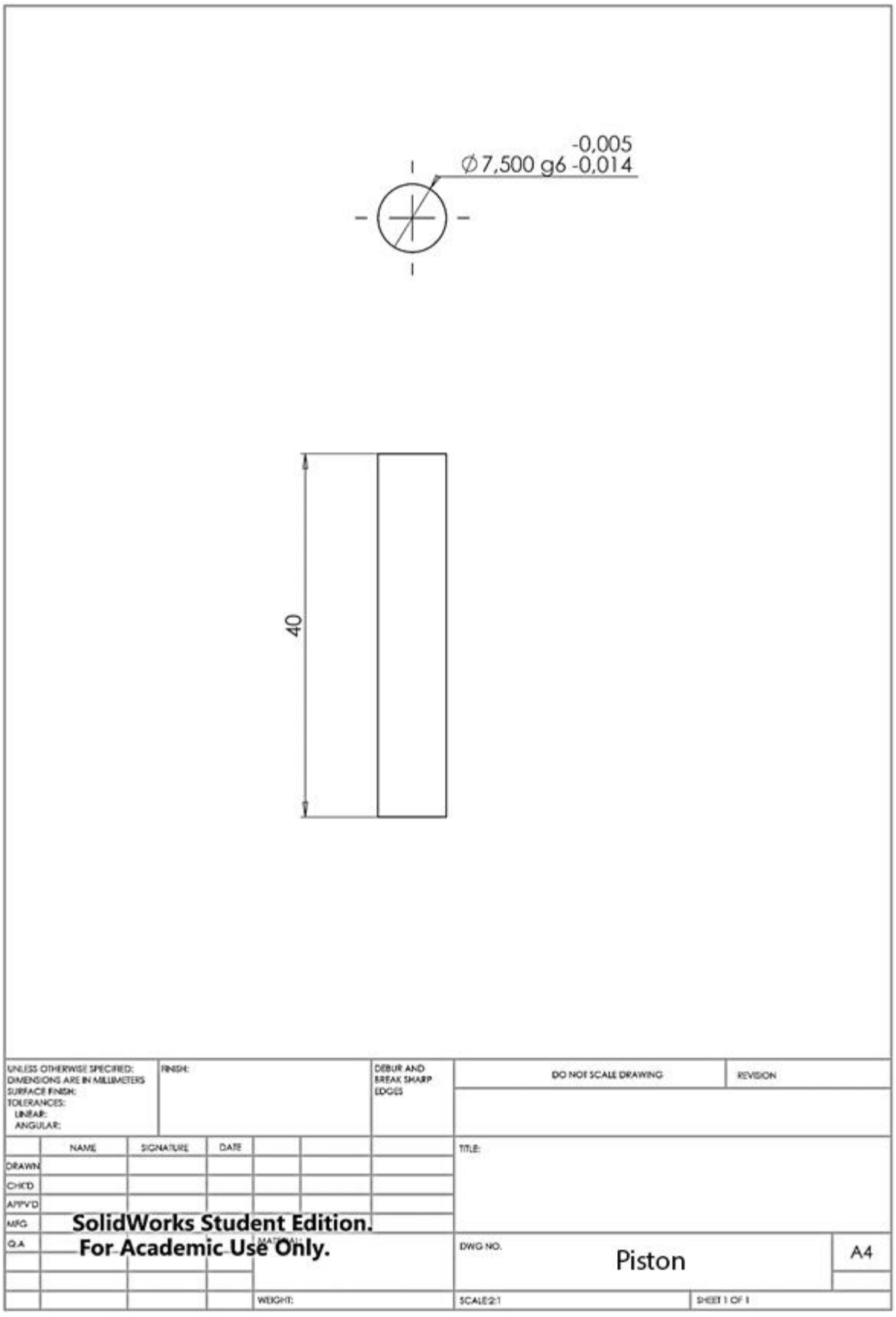
-0,005
Ø7,500 g6 -0,014
40
UNLESS OTHERWISE SPECIFIED:
DIMENSIONS ARE IN MILLIMETERS
SURFACE FINISH:
TOLERANCES:
LINEAR:
ANGULAR:
FINISH:
DEBUR AND BREAK SHARP EDGES
DO NOT SCALE DRAWING
REVISION
NAME
SIGNATURE
DATE
DRAWN
CHK'D
APP'V'D
MFG
Q.A
TITLE:
SolidWorks Student Edition.
For Academic Use Only.
DWG NO.
Piston
A4
WEIGHT:
SCALE:2:1
SHEET 1 OF 1

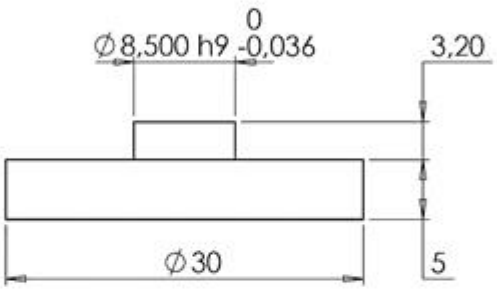

UNLESS OTHERWISE SPECIFIED: DIMENSIONS ARE IN MILLIMETERS SURFACE FINISH: TOLERANCES: LINEAR: ANGULAR:		FINISH:			DEBUR AND BREAK SHARP EDGES	DO NOT SCALE DRAWING	REVISION
	NAME	SIGNATURE	DATE			TITLE:	
DRAWN							
CHK'D							
APPVD							
MFG							
Q.A				MATERIAL		DWG NO. lid	A4
				WEIGHT:		SCALE:5:1	SHEET 1 OF 1

ANNEX B

The 2-D drawings of the target are presented in the following pages. The target can hold a sample of circular shape with 8.5 mm diameter. It is prepared for proves with 1.2 mm diameter. The design was made in order for all the part to be manufactured in a laser cutter machine with quick and low cost production.

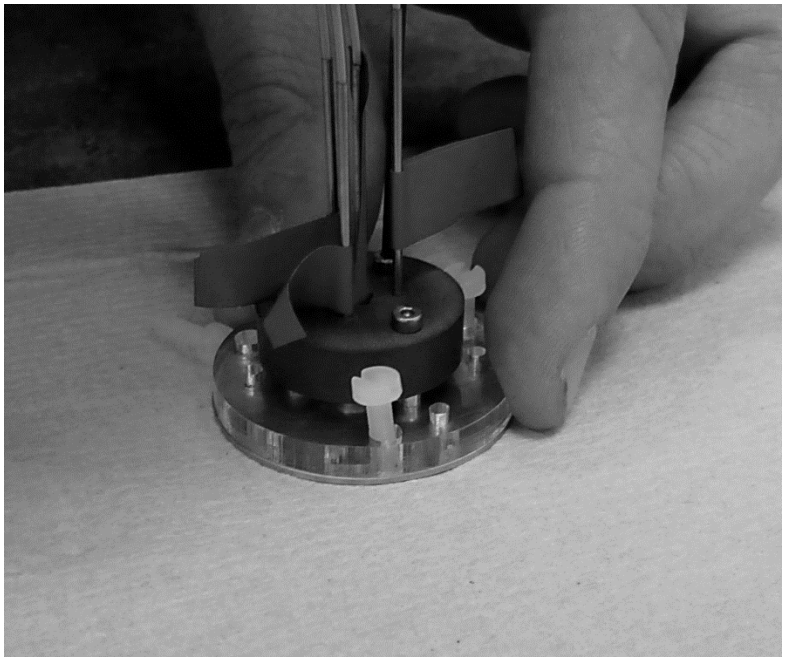

Window

Target Back 1

Target Back 2

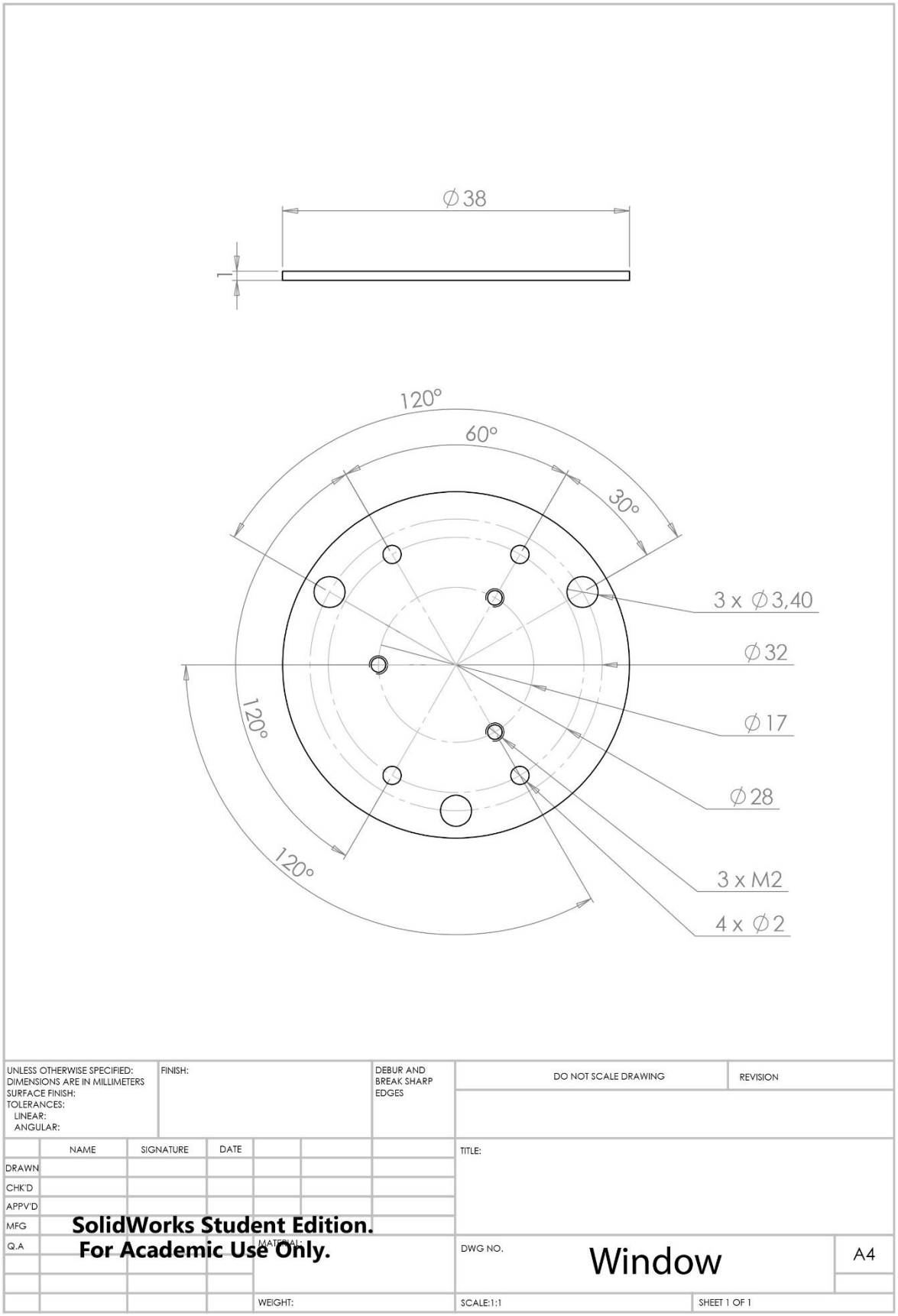
∅38
1
120°
60°
30°
3 x ∅3,40
∅32
∅17
∅28
3 x M2
4 x ∅2
120°
120°
UNLESS OTHERWISE SPECIFIED:
DIMENSIONS ARE IN MILLIMETERS
SURFACE FINISH:
TOLERANCES:
LINEAR:
ANGULAR:
FINISH:
DEBUR AND BREAK SHARP EDGES
DO NOT SCALE DRAWING
REVISION
NAME
SIGNATURE
DATE
DRAWN
CHK'D
APPV'D
MFG
Q.A
TITLE:
SolidWorks Student Edition.
For Academic Use Only.
MATERIAL:
DWG NO.
Window
A4
WEIGHT:
SCALE:1:1
SHEET 1 OF 1

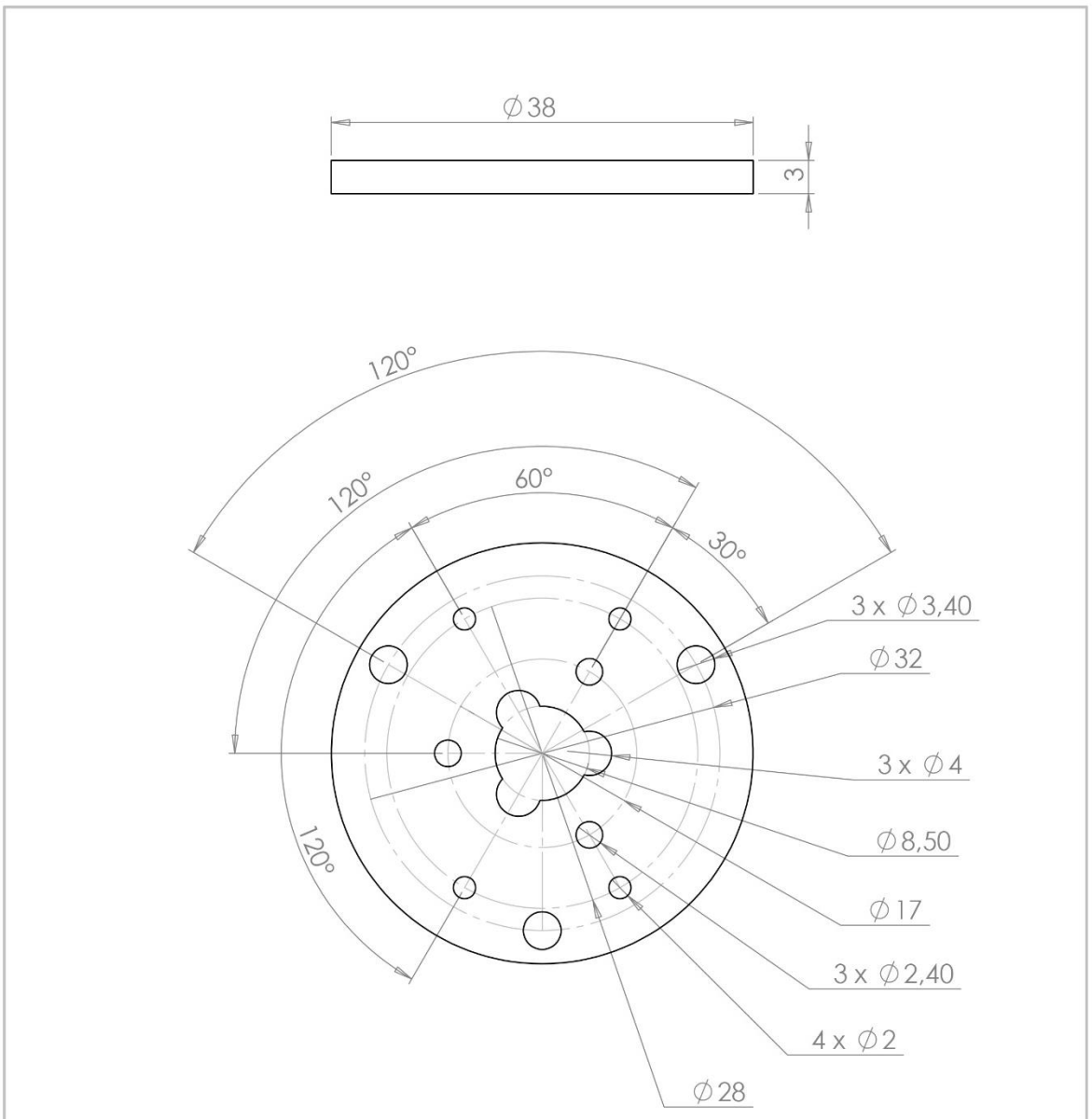

UNLESS OTHERWISE SPECIFIED: DIMENSIONS ARE IN MILLIMETERS SURFACE FINISH: TOLERANCES: LINEAR: ANGULAR:		FINISH:			DEBUR AND BREAK SHARP EDGES		DO NOT SCALE DRAWING	REVISION
	NAME	SIGNATURE	DATE				TITLE:	
DRAWN								
CHK'D								
APPV'D								
MFG								
Q.A				MATERIAL:			DWG NO. Target Back 1	A4
				WEIGHT:			SCALE:2:1	SHEET 1 OF 1

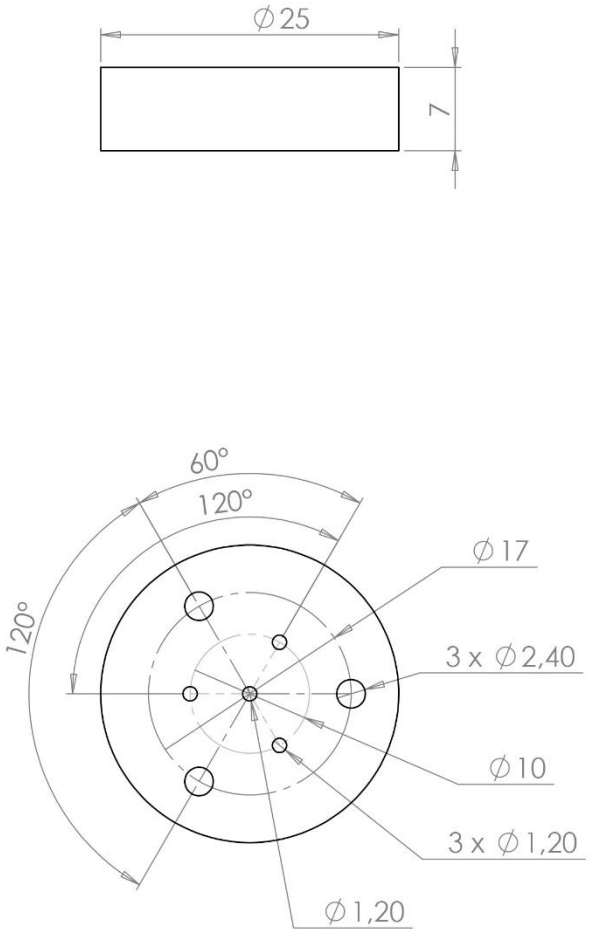

UNLESS OTHERWISE SPECIFIED: DIMENSIONS ARE IN MILLIMETERS SURFACE FINISH: TOLERANCES: LINEAR: ANGULAR:		FINISH:			DEBUR AND BREAK SHARP EDGES		DO NOT SCALE DRAWING	REVISION
	NAME	SIGNATURE	DATE				TITLE:	
DRAWN								
CHK'D								
APPV'D								
MFG								
Q.A				MATERIAL:			DWG NO.	A4
							Target Back 2	
				WEIGHT:			SCALE:2:1	SHEET 1 OF 1